RAMAN SCATTERING OF CUPRIC OXIDE (CuO)

by

Tao Wei

B.Sc. Peking University 1983

M.Sc. Peking University 1986

THESIS SUBMITTED IN PARTIAL FULFILLMENT OF

THE REQUIREMENTS FOR THE DEGREE OF

MASTER OF SCIENCE

in the Department

of

Physics

SIMON FRASER UNIVERSITY

DECEMBER 1990

APPROVAL

NAME: Tao Wei

DEGREE: Master of Science (Physics)

TITLE OF THESIS: Raman Scattering of Cupric Oxide

EXAMINING COMMITTEE:

Chairman: Dr. E. D. Crozier

Dr. J. C. Irwin
Senior Supervisor

Dr. R. F. Frindt

Dr. K. E. Rieckhoff

Dr. A. E. Curzon
Examiner

DATE APPROVED: 25 January, 1991

PARTIAL COPYRIGHT LICENSE

I hereby grant to Simon Fraser University the right to lend my thesis, project or extended essay (the title of which is shown below) to users of the Simon Fraser University Library, and to make partial or single copies only for such users or in response to a request from the library of any other university, or other educational institution, on its own behalf or for one of its users. I further agree that permission for multiple copying of this work for scholarly purposes may be granted by me or the Dean of Graduate Studies. It is understood that copying or publication of this work for financial gain shall not be allowed without my written permission.

Title of Thesis/Project/Extended Essay

Raman Scattering of Cupric Oxide (CuO)

Author: _____ _____
(Signature)

Tao Wei
(Name)

February 5, 1991
(Date)

ABSTRACT

Raman scattering experiments have been carried out on CuO crystals and $Cu^{18}O$ powder pellets in the spectral region 100-6000 cm^{-1}. Three of the observed peaks have been identified as the first order phonon scattering and their symmetries have been determined. To interpret the observed frequencies from CuO crystals, a Valence-Force-Field (VFF) lattice dynamical model for CuO is introduced and its parameters are adjusted to reproduce the experimentally measured frequencies. The eigenvectors for the vibrational modes are calculated and compared with group theoretical predictions. The model has been used to calculate the phonon frequencies of ^{18}O isotope substituted CuO and the values obtained are in excellent agreement with the observed results. The force constants obtained are found to be qualitatively consistent with two other CuO dynamical models. A comparison with equivalent bonds in high-T_c materials has also been made.

A relatively broad peak at 1100 cm^{-1} has been revealed to be two-phonon scattering by comparing Raman spectra obtained from CuO and $Cu^{18}O$. The profile and energy of the feature are in agreement with what would be expected from neutron scattering measurements of the phonon density of states.

At low temperatures a very broad feature centered at about 2200cm^{-1} is observed in Raman spectra of CuO and $Cu^{18}O$. Its frequency and lineshape are very similar to the two-magnon scattering peaks observed in the undoped high-T_c cuprates. Ascribing it to two-magnon scattering from a three-dimensional spin system is consistent with our experimental results, but it is also possible that this peak arises in part from intraband or interband electronic scattering.

ACKNOWLEDGEMENT

I gratefully acknowledge the financial support provided by Physics Department of Simon Fraser University and by my supervisor J. C. Irwin.

I wish to thank Dr. Irwin, who supervised and encouraged this research. I would also like to thank E. Altendorf, S. Jimènez Sandoval, W. McMullan, Per Joensen and J. Chrzanowski for their help and suggestions.

CONTENTS

LIST OF TABLES

LIST OF FIGURES

1. INTRODUCTION

Since the discovery of the high-temperature superconductivity in layered copper oxide compounds in late 1986 (Bednorz and Müller 1986), an enormous amount of research has been carried out on these remarkable materials.

A common feature of the currently known cuprate based high-temperature superconductors is the presence of CuO_2 planes with a square, or nearly square lattice (Ginsberg 1989). It is now widely accepted that the interactions between copper and oxygen atoms in this plane are fundamental to the superconductivity of high-T_c cuprates. Because the structure of high T_c materials is quite complex, the study of a simpler compound with similar interactions is suggested. In CuO, there also exist (Åsbrink and Norrby 1970) slightly distorted planar squares, that is, parallelograms, formed by copper and oxygen atoms. The parallelograms link together to form ribbons which extend in the [110] and [$\bar{1}$10] directions of the crystal. A copper atom is situated at the centre of each parallelogram and the distances between it and the four neighboring oxygen atoms are about 1.95Å and 1.96Å, which is comparable to the Cu-O separation of 1.90Å in the CuO_2 planes of La_2CuO_4, 1.96Å and 1.95Å respectively for the analogous bond length in the superconductor $YBa_2Cu_3O_7$ and its parent material $YBa_2Cu_3O_6$. Therefore CuO provides a similar but simpler reference frame for the study of the Cu-O interactions that appear to be so important in high T_c superconductors.

The Raman spectra from CuO pressed pellets have been investigated by Chrzanowski and Irwin (1989) and Irwin et al. (1990). Three of the observed features were assigned to first order phonon scattering and another was tentatively related to magnetic excitations. To confirm their assignments and identify the symmetries of scattering peaks, with which the interactions among atoms may be treated in more detail, further study is needed. According to the theory of Raman scattering from phonons in crystals (Loudon 1964), the intensity of the polarized Raman scattering from a phonon of certain symmetry is determined by the corresponding Raman tensor and the symmetries of the Raman tensor can be derived from the symmetry of the relevant crystal. By properly arranging the polarization configuration during measurements, the symmetries of the Raman active phonons may be obtained. Therefore we have undertaken the polarized study of Raman scattering in CuO crystals.

Once the symmetries and frequencies of all phonons are known, it is possible to interpret the atomic interactions with a suitable lattice dynamics model. In this work this has been done with a Valence Force Field (VFF) model which has been used to calculate the phonon frequencies at the center of the Brillouin zone. The model parameters have been determined using the measured Raman frequencies and using data from infrared experiments. To further corroborate the previous assignments (Chrzanowski and Irwin 1989), and also test the validity of the VFF model for CuO, Raman spectra of $Cu^{18}O$ were also measured and

compared to the results in CuO (in this thesis, CuO stands for $Cu^{16}O$) and to the predictions of the VFF model. In carrying out this comparison it is assumed that, when one type of atoms is substituted by isotopic atoms, the interactions in a material remain unchanged and that the shift of phonon frequencies is only due to the change in mass.

The magnetic interactions in CuO are also of interest. It has been widely assumed that the BCS theory based on phonon-induced pairing can not account for the large critical temperatures of high-T_c materials and other possible pairing mechanisms such as magnetic excitations have been suggested (Miller 1988, Markert et al. 1989). This possibility has led to experimental work on the magnetic interactions of Cu^{2+} ions which are present in high T_c cuprates. Raman scattering experiments (Lyons et al. 1988 (1) and (2)) have revealed a high frequency scattering which peaks at about $3000cm^{-1}$ in undoped La_2CuO_4 and $2600cm^{-1}$ in $YBa_2Cu_3O_6$, which was ascribed to two-magnon scattering on the basis of polarized experimental results. The observed peak energy yielded a large value for the exchange constant of $J\cong1100cm^{-1}$ for La_2CuO_4 and $J\cong950cm^{-1}$ for $YBa_2Cu_3O_6$. Later study however showed that other electronic excitations might also contribute to this scattering (Lyons et al. 1989), indicating that further study is needed.

CuO is also a system containing strongly interacting Cu^{2+} ions arranged in a much simpler structure. Neutron scattering experiments (Ain et al. 1988) have revealed that, for temperatures below 225K, the

Cu^{2+} moments in CuO are ordered antiferromagnetically along the [10$\bar{1}$] direction with an effective exchange constant of J≅650cm^{-1}. This value is comparable to that of high-T_c materials and thus it is expected that a study of these excitations in CuO could yield worthy information.

This thesis consists of 5 chapters. In Chapter 2, the structure of CuO is described and a brief description of the Valence Force Field (VFF) model is presented. The theoretical treatment of Raman scattering in CuO is also given in Chapter 2. Chapter 3 describes the experimental setup in detail and Chapter 4 presents the experimental results, together with analyses and discussions. Chapter 5 contains the conclusions and suggestions for further work.

2. THE RAMAN EFFECT IN CuO

1) Crystal structure of CuO

The structure of CuO is monoclinic with C_{2h}^6 (C2/c, no.15) symmetry. There are four molecular units in the crystallographic unit cell (Åsbrink and Norrby 1970). The dimensions of the unit cell are a=4.6837 Å, b=3.4226 Å, c=5.1288 Å and β=99.5°, where β is the angle between a and c axes, as shown in Fig.2.1 and Fig.2.2. The copper ions occupy symmetry sites 4(c): (1/4,1/4,0), (3/4,1/4,1/2), (3/4,3/4,0) and (1/4,3/4,1/2), which are the sites with inversion symmetry (C_i). The oxygen atoms occupy sites 4(e) at: (0,y,1/4), (0,$\bar{y}$,3/4), (1/2,1/2+y,1/4) and (1/2,1/2-y,3/4), with y=0.4184. These sites have symmetry C_2 when the rotation is taken about the two-fold b axis (Fig.2.2).

The whole structure of CuO can be viewed as shown in Fig.2.3: Every oxygen atom has four nearest copper neighbors in a distorted tetrahedral configuration. The copper atom is coordinated to four coplanar oxygen atoms situated at the corners of an almost rectangular parallelogram. The parallelograms form two ribbons, one runs in the [110] direction and another in the [$\bar{1}$10] direction. Two types of ribbons are piled alternately in the [001] direction. Each type of ribbon is stacked in the [010] direction with a separation of about 2.7Å.

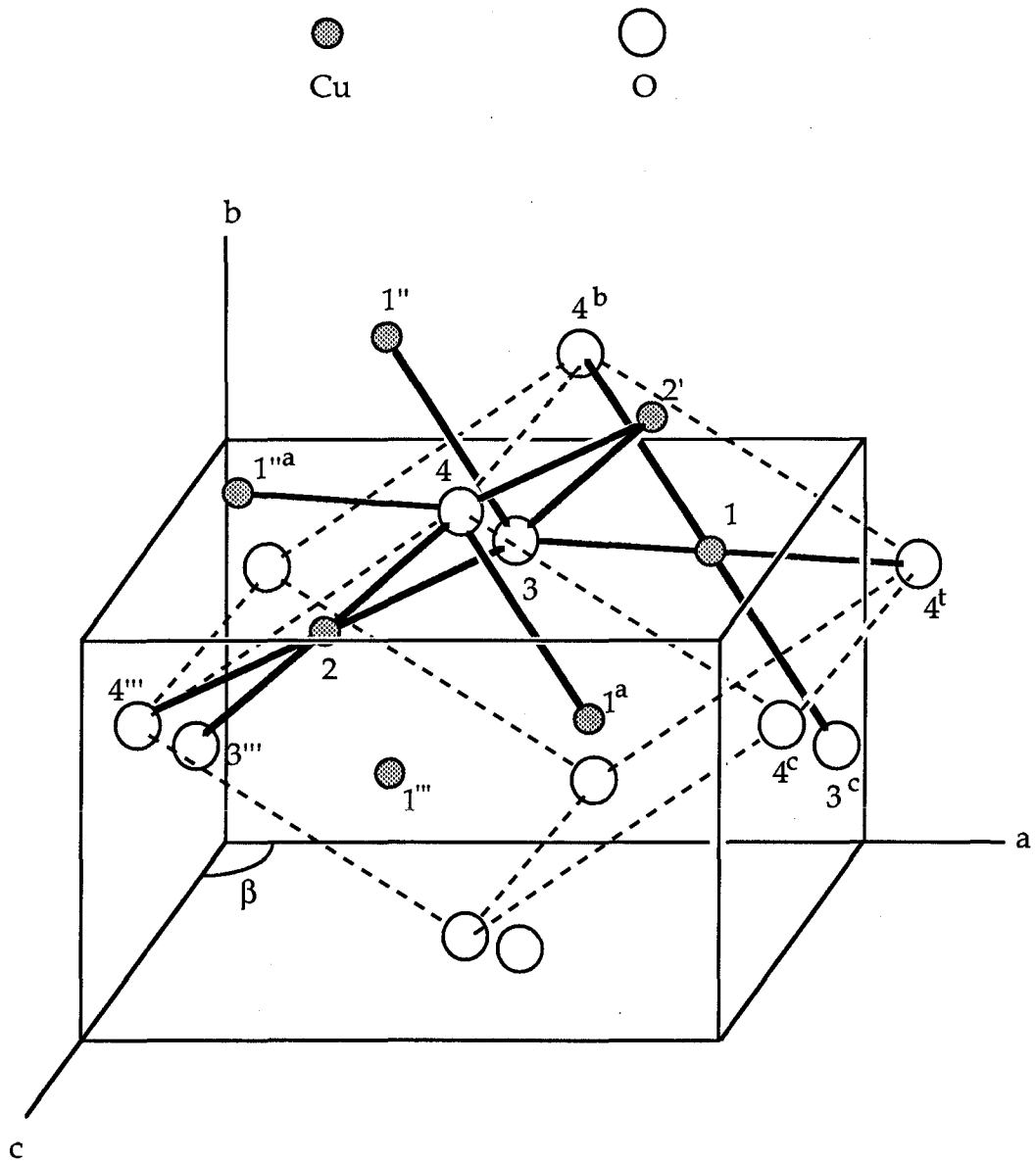

Fig. 2.1 Unit cell of CuO. The primitive cell is indicated by dashed lines. Atoms in the primitive cell are denoted by 1, 2, 3 and 4 and equivalent atoms are designated with the same number with a superscript.

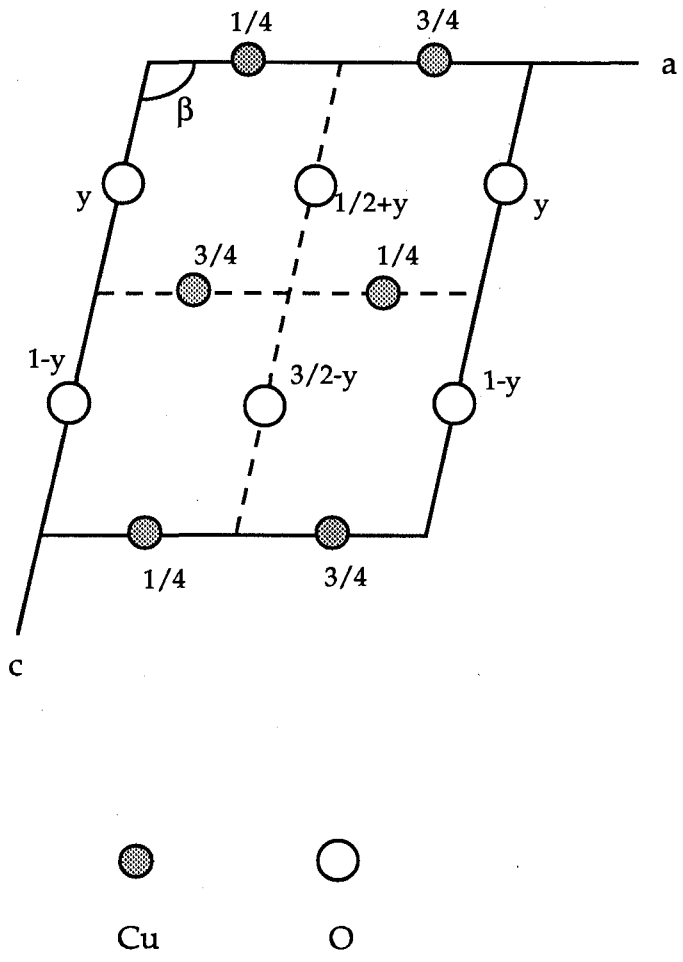

Fig. 2.2 Positions of atoms in the monoclinic unit cell of CuO. Numbers affiliated to atoms indicate elevations.

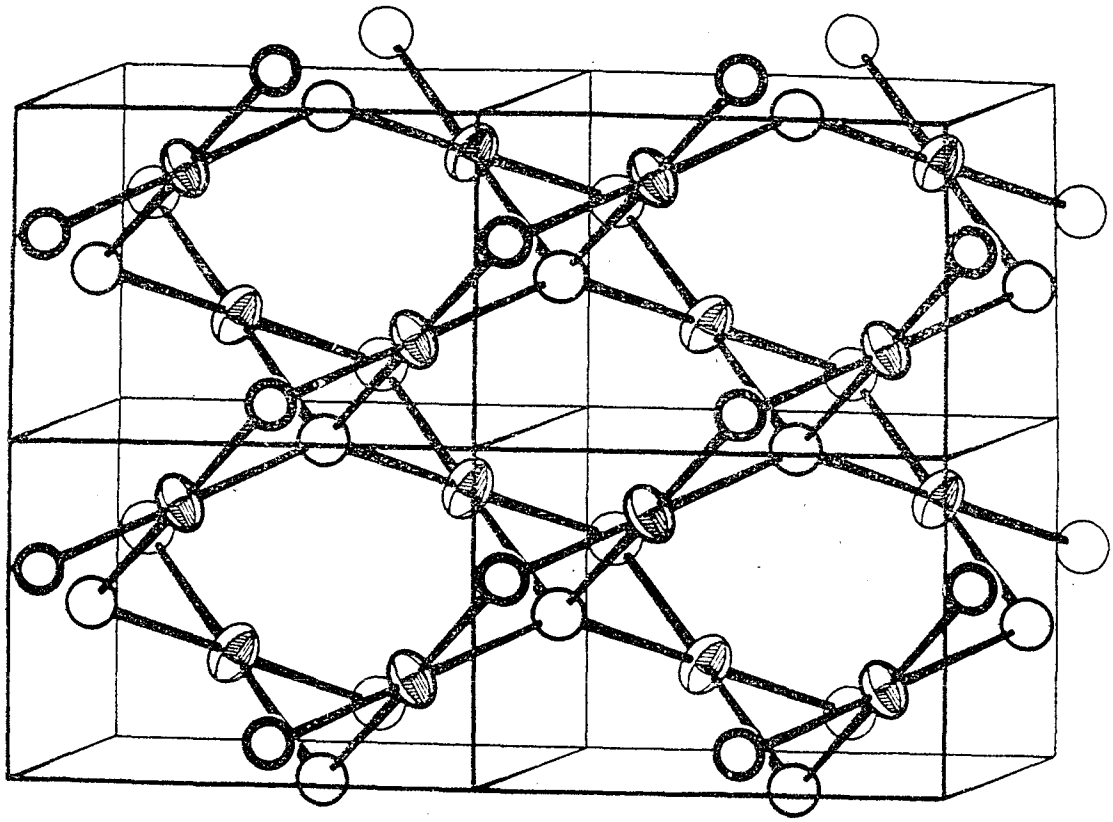

Fig. 2.3 A perspective view showing the chains of oxygen coordination parallelograms in CuO and the way in which they are linked together. From Åsbrink and Norrby(1970).

The primitive unit cell contains two molecular units, that is, 2 copper ions and 2 oxygen ions, and it is shown by the dashed lines in Fig.2.1. The atoms in the primitive cell are labeled by number 1,2,3 and 4. Other equivalent atoms are denoted by the same number with a superscript. The superscripts a, b, c, t, ', ", "' and "^{a} denote the particular primitive cell in which the atom is contained.

2)Lattice dynamics

The basic theory of lattice vibrations of a three dimensional system is given by, for example, Born and Huang (1954). In the adiabatic and harmonic approximations, that is, neglecting the electron effects on lattice vibrations and assuming small amplitude vibrations the potential energy Φ of the crystal may be expressed as (see Born and Huang 1954, Cochran 1966, or Brüesch 1982, for example)

$$2\Phi = \sum_{l\kappa\alpha} \sum_{l'\kappa'\beta} \phi_{\alpha\beta}(l\kappa, l'\kappa') u_{\alpha}(l\kappa) u_{\beta}(l'\kappa') \qquad (2.1)$$

where l identifies a primitive unit cell, κ the particular atom in the cell and u_{α} the α-component of displacements (α=x,y and z). The equilibrium position of atom κ in cell l is denoted by

$$\mathbf{r}(l\kappa) = \mathbf{r}(l) + \mathbf{r}(\kappa) \qquad (2.2)$$

The harmonic force constants are given by the second derivative of Φ

$$\phi_{\alpha\beta}(l\kappa, l'\kappa') = \left(\frac{\partial^2 \Phi}{\partial u_{\alpha}(l\kappa) \partial u_{\beta}(l'\kappa')} \right)_0 \qquad (2.3)$$

Where the index κ runs from 1 to n, and n is the number of atoms in the

primitive cell. For a crystal with N primitive cells, the number of independent coordinates is 3nN.

The equation of motion for atom (l,κ) $(\alpha, \beta=x, y, z)$

$$m_\alpha\left(\frac{\partial^2}{\partial t^2} u_\alpha(l\kappa)\right)=-\sum_{l'\kappa'\beta} \phi_{\alpha\beta}(l\kappa,l'\kappa')u_\beta(l'\kappa') \tag{2.4}$$

is formally solved by introducing the following form of solution,

$$u_\alpha(l\kappa)=U_\alpha(\kappa,q)\exp i(q\cdot r(l\kappa)-\omega(q)t) \tag{2.5}$$

as a plane wave travelling in the direction of the wave vector q, where $U_\alpha(\kappa,q)$ is the α-component of the amplitude. The equations of motion then become

$$\omega^2(q)m_\kappa U_\alpha(\kappa,q)=\sum_{\kappa'\beta} M(\kappa\alpha,\kappa'\beta,q)U_\beta(\kappa',q) \tag{2.6}$$

where

$$M(\kappa\alpha,\kappa'\beta,q)=\sum_{l'} \phi_{\alpha\beta}(l\kappa,l'\kappa')\exp iq\cdot(r(l'\kappa')-r(l\kappa)) \tag{2.7}$$

The condition that the equations have non-trivial solutions is

$$\mathrm{Det}\ [M(\kappa\alpha,\kappa'\beta,q)-\delta_{\alpha\beta}\delta_{\kappa\kappa'}m_\kappa\omega^2]=0 \tag{2.8}$$

The 3n×3n matrix $M(\kappa\alpha,\kappa'\beta',q)$ is known as the dynamical matrix. There are 3n solutions $\omega(q)$ for each q, written as $\omega_j(q)(j=1,2,\cdots,3n)$, and corresponding wave amplitudes or eigenvectors $U(\kappa,q,j)$. $\omega_j(q)$ are the frequencies of the normal modes of vibrations $u_j(l,\kappa)$ of the crystal. In the language of quantum mechanics $\omega_j(q)$ are the frequencies of phonons with wave vector q, as can be seen when proper creation and annihilation operators are introduced and the Hamiltonian of the crystal

is quantized (see Maradudin 1974 for details). For CuO which has 4 atoms in the primitive cell, there are 12 normal modes or 12 phonon branches for every value of the wave vector **q**.

Eq.(2.7) and (2.8) show that the problem in interpreting phonon dispersion relationships therefore is to find force constants $\phi_{\alpha\beta}(l\kappa,l'\kappa')$ which will account for the measured frequencies and dispersion of phonons and possibly yield an interpretation of the force constants in terms of known interactions.

3) Force constants

As we will see in Section 2.5, only phonons with wavevector $\mathbf{q}\approx 0$ are involved in the first order Raman scattering. Thus to compare with the Raman data from the CuO crystal, we need to consider the lattice dynamics at $\mathbf{q}=0$ only. In this case the elements of the dynamical matrix Eq.(2.7) are simplified as

$$M(\kappa\alpha,\kappa'\beta)\equiv M(\kappa\alpha,\kappa'\beta,\mathbf{q}=0)=\sum_{l'}\phi_{\alpha\beta}(l\kappa,l'\kappa') \qquad (2.9)$$

The symmetry operations of the CuO lattice place certain restrictions on the form of the force constant matrix $[\phi(l\kappa,l'\kappa')]_{3\times3}$. With the x and y axes chosen to lie along the a and b crystal axes, respectively, the force constant matrices, for example $\phi(3,1)\equiv[\phi(l3,l1)]_{3\times3}$ and $\phi(4,1''^{a})\equiv[\phi(l4,l''^{a}1)]_{3\times3}$ (here $l3$, $l1$ and $l4$

are atom number 3, 1, and 4 in the primitive cell labelled by *l* and *l*"^{a}1 is atom 1 in cell *l*"^{a} (Fig.2.1)), must obey the forms:

$$-\phi(3,1)=\begin{pmatrix} \alpha_{11} & \alpha_{12} & \alpha_{13} \\ \alpha_{21} & \alpha_{22} & \alpha_{23} \\ \alpha_{31} & \alpha_{32} & \alpha_{33} \end{pmatrix}=-\phi(4,1"^{a}) \tag{2.10a}$$

where α_{ij} are arbitrary parameters. Details of calculations are given in Appendix 1. For other force constants between the first and second nearest neighbors, we have (atom positions are shown in Fig.2.1)

$$-\phi(3,2)=\begin{pmatrix} \alpha_{11} & -\alpha_{12} & \alpha_{13} \\ -\alpha_{21} & \alpha_{22} & -\alpha_{23} \\ \alpha_{31} & -\alpha_{32} & \alpha_{33} \end{pmatrix}=-\phi(4,2') \tag{2.10b}$$

$$-\phi(3,1")=\begin{pmatrix} \beta_{11} & \beta_{12} & \beta_{13} \\ \beta_{21} & \beta_{22} & \beta_{23} \\ \beta_{31} & \beta_{32} & \beta_{33} \end{pmatrix}=-\phi(4,1^{a}) \tag{2.10c}$$

$$-\phi(3,2')=\begin{pmatrix} \beta_{11} & -\beta_{12} & \beta_{13} \\ -\beta_{21} & \beta_{22} & -\beta_{23} \\ \beta_{31} & -\beta_{32} & \beta_{33} \end{pmatrix}=-\phi(4,2) \tag{2.10d}$$

$$-\phi(3,4)=\begin{pmatrix} \delta_{11} & \delta_{12} & \delta_{13} \\ \delta_{12} & \delta_{22} & \delta_{23} \\ \delta_{13} & \delta_{23} & \delta_{33} \end{pmatrix} \tag{2.10e}$$

$$-\phi(3,4^{a})=\begin{pmatrix} \delta_{11} & -\delta_{12} & \delta_{13} \\ -\delta_{12} & \delta_{22} & -\delta_{23} \\ \delta_{13} & -\delta_{23} & \delta_{33} \end{pmatrix} \tag{2.10f}$$

$$-\phi(1,2')=\begin{pmatrix} \eta_{11} & \eta_{12} & \eta_{13} \\ \eta_{21} & \eta_{22} & \eta_{23} \\ \eta_{31} & \eta_{32} & \eta_{33} \end{pmatrix}=-\phi(1,2^{t}) \tag{2.10g}$$

$$-\phi(1,2^{c})=\begin{pmatrix} \eta_{11} & -\eta_{21} & \eta_{31} \\ -\eta_{12} & \eta_{22} & -\eta_{32} \\ \eta_{13} & -\eta_{23} & \eta_{33} \end{pmatrix}=-\phi(1,2'^{b}) \tag{2.10h}$$

here β_{ij}, δ_{ij} and η_{ij} are arbitrary parameters.

By defining $$\gamma_{ij}\equiv\alpha_{ij}+\beta_{ij} \tag{2.11}$$

and using the properties such as (see Appendix 1)

$$-\phi(l\kappa,l'\kappa')=-\tilde{\phi}(l'\kappa',l\kappa) \tag{2.12}$$

and

$$M(\kappa\alpha,\kappa'\beta)= -\sum_{\kappa'\neq\kappa} M(\kappa\alpha,\kappa'\beta) \tag{2.13}$$

We obtain, for q=0, the full dynamical matrix M including nearest and next nearest neighbor interactions as

$$M=\begin{pmatrix} A & C \\ \tilde{C} & B \end{pmatrix} \tag{2.14}$$

where A, B and C are 6×6 matrices and they are shown in Table 2.1.

Because of the symmetry properties of the crystal, this form of matrix is also correct when additional, for example, the third neighbor, interactions are taken into account (see Appendix 1).

In addition, applying properties (2.12) and (2.13) to Eq.(2.7), one can see that the matrix M is always hermitian and at q=0 it is real and symmetric, so the following conditions must be satisfied:

$$\gamma_{21}=\gamma_{12}+\eta_{12}-\eta_{21} \tag{2.15a}$$

$$\gamma_{32}=\gamma_{23}+\eta_{23}-\eta_{32} \tag{2.15b}$$

$$\gamma_{31}=\gamma_{13} \tag{2.15c}$$

To extract more direct physical meaning from ϕ which represents the mix of interactions among atoms, further details of the interatomic interactions must be considered. One of the methods of considering interatomic interactions is dividing them into two parts (somewhat

Table 2.1 The matrices A, B and C in the dynamical matrix M of CuO.

$$A=\begin{bmatrix}
2\gamma_{11}+4\eta_{11} & 2\gamma_{21}-(\eta_{12}-\eta_{21}) & 2\gamma_{31}+2(\eta_{13}+\eta_{31}) & -4\eta_{11} & \eta_{12}-\eta_{21} & -2(\eta_{13}+\eta_{31}) \\
2\gamma_{12}+\eta_{12}-\eta_{21} & 2\gamma_{22}+4\eta_{22} & 2\gamma_{32}-(\eta_{23}-\eta_{32}) & -(\eta_{12}-\eta_{21}) & -4\eta_{22} & \eta_{23}-\eta_{32} \\
2\gamma_{13}+2(\eta_{13}+\eta_{31}) & 2\gamma_{23}+\eta_{23}-\eta_{32} & 2\gamma_{33}+4\eta_{33} & -2(\eta_{13}+\eta_{31}) & -(\eta_{23}-\eta_{32}) & -4\eta_{33} \\
-4\eta_{11} & -(\eta_{12}-\eta_{21}) & -2(\eta_{13}+\eta_{31}) & 2\gamma_{11}+4\eta_{11} & -2\gamma_{21}+\eta_{12}-\eta_{21} & 2\gamma_{31}+2(\eta_{13}+\eta_{31}) \\
\eta_{12}-\eta_{21} & -4\eta_{22} & -(\eta_{23}-\eta_{32}) & -2\gamma_{12}-(\eta_{12}-\eta_{21}) & 2\gamma_{22}+4\eta_{22} & -2\gamma_{32}+\eta_{23}-\eta_{32} \\
-2(\eta_{13}+\eta_{31}) & \eta_{23}-\eta_{32} & -4\eta_{33} & 2\gamma_{13}+2(\eta_{13}+\eta_{31}) & -2\gamma_{23}-(\eta_{23}-\eta_{32}) & 2\gamma_{33}+4\eta_{33}
\end{bmatrix}$$

$$B=\begin{bmatrix}
2(\gamma_{11}+\delta_{11}) & & 2(\gamma_{13}+\delta_{13}) & -2\delta_{11} & & -2\delta_{13} \\
& 2(\gamma_{22}+\delta_{22}) & & & -2\delta_{22} & \\
2(\gamma_{31}+\delta_{13}) & & 2(\gamma_{33}+\delta_{33}) & -2\delta_{13} & & -2\delta_{33} \\
-2\delta_{11} & & -2\delta_{13} & 2(\gamma_{11}+\delta_{11}) & & 2(\gamma_{13}+\delta_{13}) \\
& -2\delta_{22} & & & 2(\gamma_{22}+\delta_{22}) & \\
-2\delta_{13} & & -2\delta_{33} & 2(\gamma_{31}+\delta_{13}) & & 2(\gamma_{33}+\delta_{33})
\end{bmatrix}$$

Table 2.1(cont.)

$$C=\begin{bmatrix} -\gamma_{11} & -\gamma_{21} & -\gamma_{31} & -\gamma_{11} & -\gamma_{21} & -\gamma_{31} \\ -\gamma_{12} & -\gamma_{22} & -\gamma_{32} & -\gamma_{12} & -\gamma_{22} & -\gamma_{32} \\ -\gamma_{13} & -\gamma_{23} & -\gamma_{33} & -\gamma_{13} & -\gamma_{23} & -\gamma_{33} \\ -\gamma_{11} & \gamma_{21} & -\gamma_{31} & -\gamma_{11} & \gamma_{21} & -\gamma_{31} \\ \gamma_{12} & -\gamma_{22} & \gamma_{32} & \gamma_{12} & -\gamma_{22} & \gamma_{32} \\ -\gamma_{13} & \gamma_{23} & -\gamma_{33} & -\gamma_{13} & \gamma_{23} & -\gamma_{33} \end{bmatrix}$$

arbitrarily): for example, short range forces and long range Coulomb interactions and then dealing with them separately.

It is known (Maradudin 1974) that in a crystal such as CuO with a centre of inversion, the atomic vibrations of a long wavelength mode with odd symmetry (which are infrared active modes, see Bruesch 1986, or the following Chapters 2.6 and 4.2) lead to the existence of a long range electric field in the crystal, which in turn enhances the bonding in the longitudinal vibration over that of the transverse optic vibration. This results in the well known Lyddane-Sachs-Teller splitting of long wavelength phonons with odd symmetry. The Coulomb interactions are not required, however, to describe vibrations with even symmetry (Raman active modes) or the transverse optic branches of the vibrations with odd symmetry. Since we are primarily interested in the Raman active modes we have omitted the Coulomb interaction from our calculation for the purpose of simplification, although the bonding in CuO presents a partially ionic nature (Reichardt et al. 1990). Only short range interactions are included in our following treatment of CuO.

One simple way of describing short range interactions is to express the potential energy in terms of bond stretching and the change of angle between bonds, which lead to the valence-force-field (VFF) model (Herzberg 1950, Wilson et al. 1955):

$$2\Phi = k_{r1} \sum_i (\Delta r_{1i})^2 + k_{r2} \sum_i (\Delta r_{2i})^2 + \cdots$$

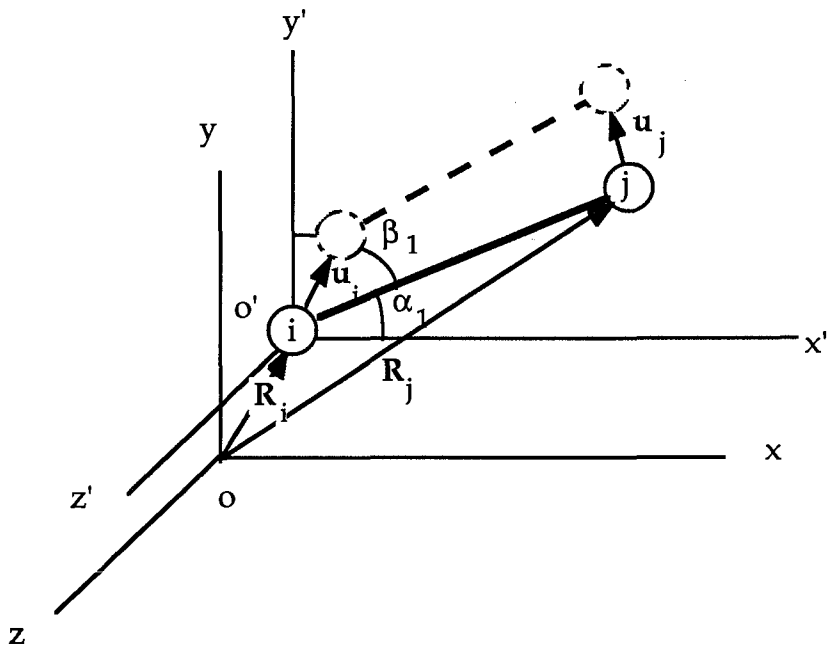

Fig. 2.4 A bond with two atoms i and j, before(solid line) and after(dashed line) a vibration.

$$+k_{\psi 1}\sum_{j} r_{1j}^{(1)}r_{2j}^{(1)}(\Delta\psi_{1j})^{2}+k_{\psi 2}\sum_{j} r_{1j}^{(2)}r_{2j}^{(2)}(\Delta\psi_{2j})^{2}+\cdots \tag{2.16}$$

where Δr_{si} are the stretch of bonds of interest and $\Delta\psi_{tj}$ are the change of the angles between bonds $r_{1j}^{(t)}$ and $r_{2j}^{(t)}$. k_{rs} are known as the stretch force constants, and $k_{\psi t}$ (or $k_{\psi t}r_{1j}^{(t)}r_{2j}^{(t)}$ used by some reference writers) as bending (or angular) force constants, s, t=1, 2, 3, ···.

With this expression of potential energy and Eq.(2.3), it is straight forward to find out force constant matrices ϕ_{ij} in cartesian coordinates and then to construct the dynamical matrix M.

Considering a spring between two atoms i and j (Fig.2.4), the stretch potential energy is Eq.(2.16)

$$\Phi=\frac{1}{2}k_{s}|\mathbf{R}_{i}-\mathbf{R}_{j}|^{2}=\frac{1}{2}k_{s}|\mathbf{u}_{i}-\mathbf{u}_{j}|^{2} \tag{2.17}$$

where $\mathbf{R}_{i}$ and $\mathbf{R}_{j}$ are positions of atoms. The force constant matrix ϕ^{s} is easy to derive with Eq.(2.3):

$$\phi^{s}=-k_{s}\begin{pmatrix} \cos^{2}\alpha_{1} & \cos\alpha_{1}\cos\beta_{1} & \cos\alpha_{1}\cos\gamma_{1} \\ \cos\alpha_{1}\cos\beta_{1} & \cos^{2}\beta_{1} & \cos\beta_{1}\cos\gamma_{1} \\ \cos\alpha_{1}\cos\gamma_{1} & \cos\beta_{1}\cos\gamma_{1} & \cos^{2}\gamma_{1} \end{pmatrix} \tag{2.18}$$

where α_{1}, β_{1} and γ_{1} are angles between the bond and cartesian axes x, y and z, respectively (Fig.2.4).

For two adjacent bonds with a bending force constant k_{ψ} (Fig.2.5), the potential energy is:

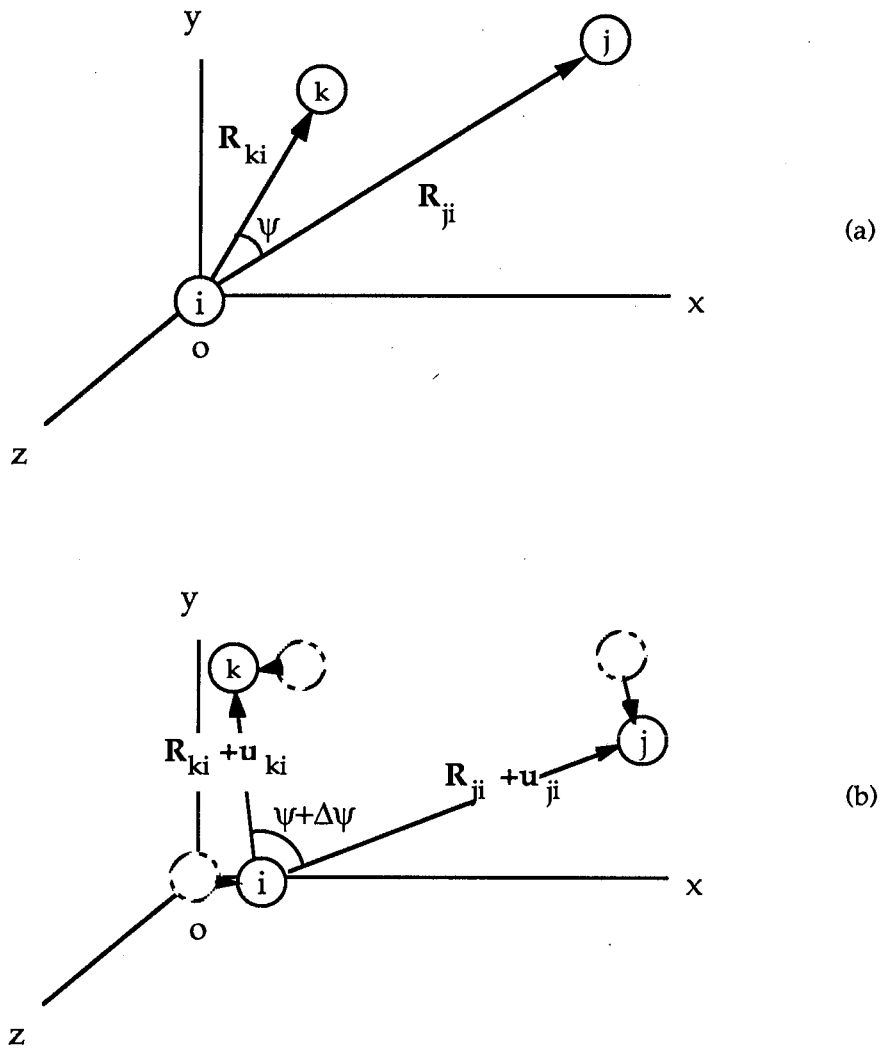

Fig. 2.5 Positions of atoms i, j and k before(a) and after (b) a bending.

$$\Phi=\frac{1}{2}k_{\psi}x_0x_0'(\Delta\psi)^2 \tag{2.19}$$

where $x_0=|R_{ji}|$ and $x_0'=|R_{ki}|$, R_{ji} and R_{ki} are equilibrium position vectors. The force constant matrix elements expressed in terms of the bending force constant k_{ψ} are (see Appendix 2 for detail calculations):

$$\phi^b_{\alpha\beta}(i,j)= - \frac{k_{\psi}}{x_0^2(1+\cos\psi_0)}(R^{\alpha}_{ki}+R^{\alpha}_{ji})(R^{\beta}_{ki}-R^{\beta}_{ji}\cos\psi_0) \tag{2.20}$$

and

$$\phi^b_{\alpha\beta}(k,j)=\frac{k_{\psi}}{x_0^2\sin\psi_0}(R^{\alpha}_{ji}-R^{\alpha}_{ki}\cos\psi_0)(R^{\beta}_{ki}-R^{\beta}_{ji}\cos\psi_0) \tag{2.21}$$

In our treatment of CuO, 6 stretch and 5 bending force constants are taken into account and their definitions are shown in Figs.2.6 and 2.7 and summarized in Table 2.2. The atom notations used by Åsbrink and Norrby are also given, since their notation is commonly used. Force constants k_1 to k_7 represent nearest neighbor interactions while the remaining stretch force constants k_8 to k_{11} are second and third nearest neighbor interactions. For all the bending force constants, k_3 to k_7, $r^{(t)}_{1j}$=1.9068Å and $r^{(t)}_{2j}$=1.9059Å, so it is easy to calculate $k_{\psi t}r^{(t)}_{1j}r^{(t)}_{2j}$ when they are desired. With the above three equations (2.19)-(2.21), the matrices used in constructing matrix M expressed in terms of k_i ($i=1,2,\cdots,11$) can be calculated and they are given as Eqs.(A2.14a, b and c) in Appendix 2.

With these expressions (Eq.(A2.14)), the frequencies of phonons can

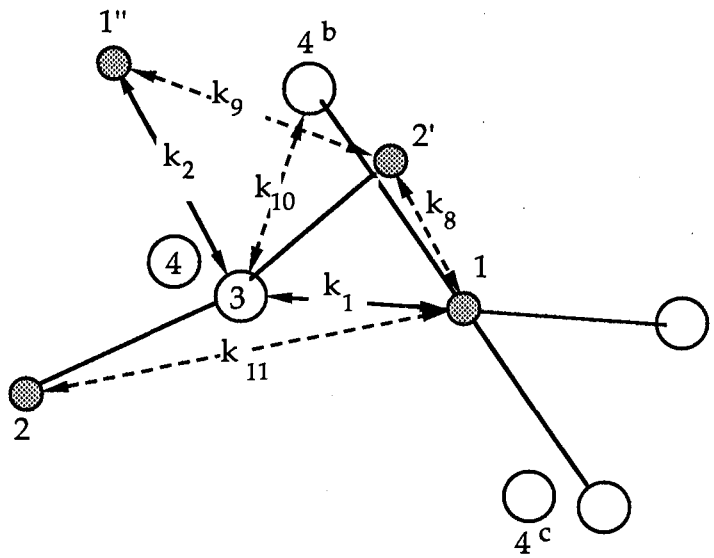

Fig. 2.6 Definitions of the stretch force constants in VFF model for CuO.

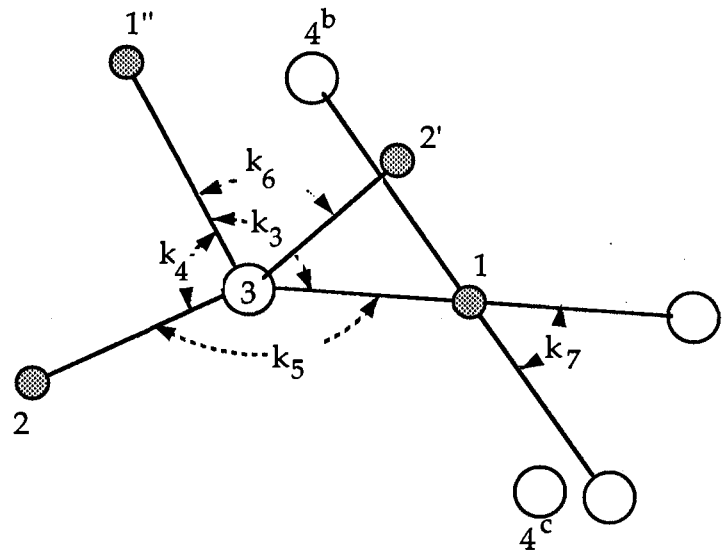

Fig. 2.7 Definitions of the bending force constants in VFF model for CuO.

Table 2.2. Definitions of the force constants for CuO.

force constant	bond type[a]	distance (Å) or angle
k_1	O3-Cu1/O-Cu(4)	1.9608
k_2	O3-Cu1"/O-Cu(ii)(4)	1.9509
k_3	Cu1-O3-Cu1"/Cu-O-Cu(ii)(4)	95.72°
k_4	Cu1"-O3-Cu2/Cu-O-Cu(iv)(4)	104.03°
k_5	Cu1-O3-Cu2/Cu-O-Cu(viii)(2)	145.82°
k_6	Cu1"-O3-Cu2'/Cu(ii)-O-Cu(iv)(2)	108.85°
k_7	O3-Cu1-Cu4[b]/O-Cu-O(v)(4)	84.28°
k_8	Cu1-Cu2'/Cu-Cu(iv)(4)	3.0830
k_9	Cu1"-Cu2'/Cu(ii)-Cu(iv)(2)	3.1734
k_{10}	O3-O4/O-O(v)(2)	2.6246
k_{11}	Cu1-Cu2/Cu-Cu(viii)(2)	3.7484

a) Following the slashes are notations adopted by Åsbrink and Norrby (1970). The number in brackets represents the number of bonds.

be calculated provided that all k_i are known. Most commonly, k_i are adjusted so that the frequencies match the experimental results, as we will do in Chapter 4.

4) Irreducible representations of phonons

For a given matrix M, a set of eigenvalues ω_j^2 with corresponding eigenvectors $U_j(l\kappa)$ can be found from Eq.(2.8). $U_j(l\kappa)$ form a complete set of vectors which can be used as a basis for the symmetry representations of ω_j^2. The representations of ω_j^2 can be further reduced into irreducible representations by means of group theory and thus used to classify the modes with frequencies ω_j^2. There is a standard group theory calculation procedure to follow (Heine 1960 and Birman 1974) and various tables have been compiled to facilitate rapid calculations (for example, Fateley et al. 1972 and Rousseau et al. 1981). With oxygen and copper atoms occupying the C_2 and C_i sites, respectively, the 12 irreducible representations of phonon branches of CuO at point q=0 (the Γ point), can be determined from Rousseau et al.'s Table 5B as (with Mulliken's notation)

$$\Gamma=4A_u+5B_u+A_g+2B_g \tag{2.22a}$$

or with Bethe's notation

$$\Gamma=4\Gamma_1^-+5\Gamma_2^-+\Gamma_1^++2\Gamma_2^+ \tag{2.22b}$$

Three modes represented by A_u+2B_u are acoustic branches, in which U_j are uniform translation displacements at q=0, and their frequencies approach

zero as q approaches zero. Thus they are not observed in a Raman spectrum.

5) Introduction of Raman effect

The Raman effect is the inelastic scattering of electromagnetic radiation by collective excitations in matter. For a crystalline medium, in the view of quantum mechanics, it is a scattering process in which a crystal excitation is created (in the Stokes process) or annihilated (in the anti-Stokes process) (Fig.2.8). These collective excitations can be optical phonons, acoustic phonons (Brillouin scattering), magnons, plasmons, etc. Studies (Loudon 1964) have shown that the most important scattering process results from the coupling of the light waves to electronic distortions of crystals. For phonons, the most important mechanism has been developed in detail by Loudon (1964). In the one-phonon case, the incident light excites a virtual electron-hole pair, e_1, which either creates or absorbs a phonon resulting in the formation of another pair e_2, which then recombines to emit the scattered photon. According to perturbation theory, the polarization amplitude of such a process is proportional to (Loudon 1964)

$$\sum_{e_1 e_2} \frac{\langle i|H_A^{\alpha}|e_1\rangle\langle e_1|H_{EL}|e_2\rangle\langle e_2|H_A^{\beta}|f\rangle}{(\omega_{e_1}-\omega_i)(\omega_{e_2}-\omega_s)} \qquad (2.23)$$

here H_A^{α} represents the coupling between photons and electrons with the

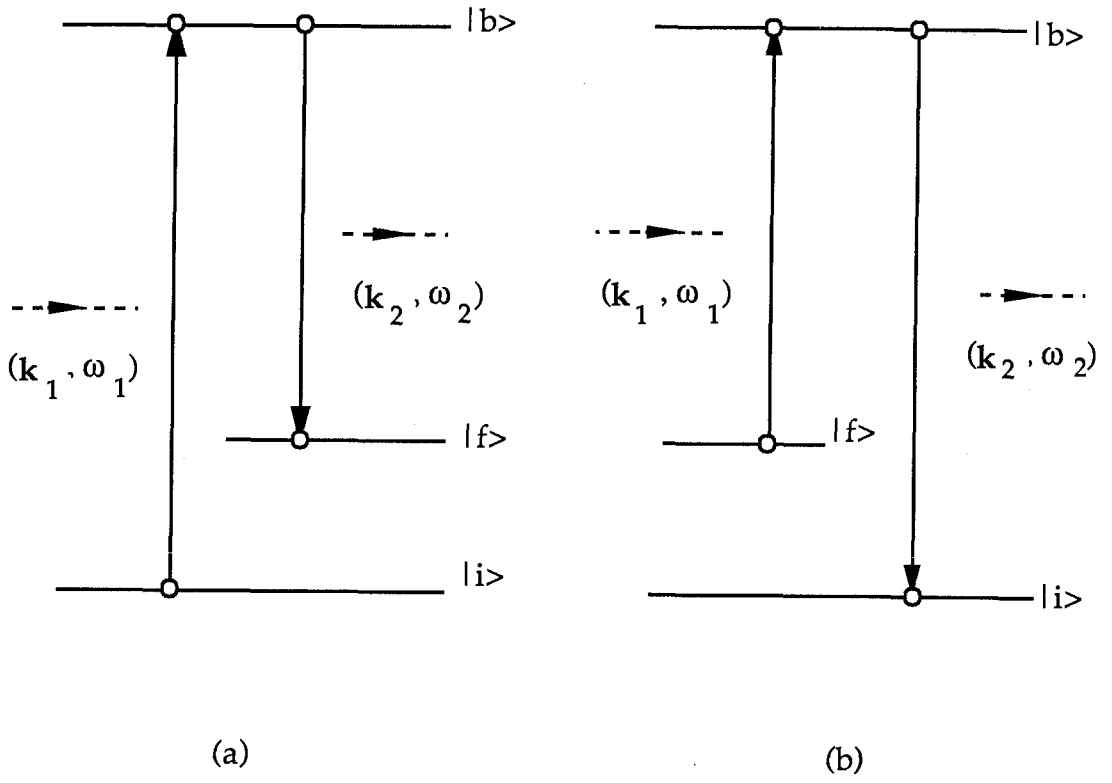

Fig. 2.8 Schematic description of transitions of Stokes process(a) and anti-Stokes process(b).

light polarized in α direction, H_{EL} represents the coupling between electrons and phonons, that is, the electron-phonon interaction. This, and other similar expressions determine the Raman scattering intensities of phonons, and thus the selection rules and Raman tensors of the crystal. Unfortunately, these calculations are very complicated and when only the selection rules are needed they may be obtained with the more phenomenological approach described in the following section.

The conservation of energy and momentum of Raman process are

$$\omega_i = \omega_s \pm \omega \tag{2.24a}$$

$$\mathbf{k}_i = \mathbf{k}_s \pm \mathbf{q} \tag{2.24b}$$

here $\mathbf{q}$ is the momentum of the phonon. + and - signs correspond to Stokes process and anti-Stokes process, respectively. Generally, the incident and scattered photon wavelengths λ_i and λ_s are much longer than the lattice constant a, so $q_{max} = k_i + k_s \ll \pi/a$, that is, $\mathbf{q}$ is very close to the centre of the Brillouin zone, or $\mathbf{q} \simeq 0$.

In a higher order Raman process, such as a two-phonon scattering process, the conservation rules may be written as

$$\omega_i = \omega_s \pm \omega_1(\mathbf{q}_1 j_1) \pm \omega_2(\mathbf{q}_2 j_2) \tag{2.25a}$$

$$\mathbf{k}_i - \mathbf{k}_s = \pm\mathbf{q}_1 \pm \mathbf{q}_2 \cong 0 \tag{2.25b}$$

One can see that in Eq.(2.25b) the wavevectors of phonons involved in the two-phonon scattering are not limited to particular points in the

Brillouin zone, and the contributions to the two-phonon spectrum may come from points throughout the Brillouin zone. The two-phonon spectrum will thus consist of a continuous background as a function of frequency with peaks arising from singularities in the density of states superimposed on the background. This is in contrast to the one phonon spectrum which usually consists of relatively sharp discrete peaks corresponding to the zone centre optical phonons (Cowley 1971). Higher order scattering of other excitations, such as magnons, also exhibit these kind of features.

From thermodynamics we know that in equilibrium the number of phonons of frequency ω is given by $\bar{n}_{\omega}=\frac{1}{e^{\hbar\omega/kT}-1}$. Studies (Sherwood 1972) have shown that, if the phonon-phonon interaction is neglected, the scattering intensity of a one-phonon Stokes process is proportional to $1+\bar{n}_{\omega}$, which increase with increasing temperature. For the higher order process such as a two phonon process with $q_1-q_2=0$, the factor becomes $\bar{n}_1\bar{n}_2+\bar{n}_2$. The factors for other higher order phonon processes have been obtained by studying these processes in detail (see Sherwood 1972, for example).

6) Selection rules

Phenomenologically, the Raman effect may be viewed as an interaction of the incident and scattered waves with the collective

excitations in the crystal.

Considering the electric field $\mathbf{E}_i = \hat{e}_i E_i$ ($\hat{e}_i$ is an unit vector) associated with an electromagnetic wave in the crystal. The induced dipole moment is

$$\mathbf{M} = \tilde{\chi} \cdot \hat{e}_i E_i \tag{2.26}$$

where $\tilde{\chi}$ is the polarizability tensor of the crystal. The radiation energy emitted per unit time by the dipole moment $\mathbf{M}$ vibrating at the frequency ω is (Landau and Lifschitz 1960):

$$\frac{dW_s}{d\Omega} = \frac{\omega^4}{(4\pi)^2 \epsilon_0 c^3} |\hat{e}_s \cdot \mathbf{M}|^2 = \frac{\omega^4 E_i}{(4\pi)^2 \epsilon_0 c^3} |\hat{e}_s \cdot \tilde{\chi} \cdot \hat{e}_i|^2 \tag{2.27}$$

where ϵ_0 is the dielectric constant (permittivity) of the crystal, c the speed of light in the crystal and $\hat{e}_s$ the unit vector representing the polarization of the scattered light.

$\tilde{\chi}$ can be expanded in Taylor series in terms of collective excitation coordinates Q_m

$$\tilde{\chi}_{\alpha\beta} = \tilde{\chi}^{(0)}_{\alpha\beta} + \tilde{\chi}^{(1)}_{\alpha\beta} + \cdots \tag{2.28}$$

$\tilde{\chi}^{(0)}$ is responsible for the elastic (Raleigh) scattering and the first order transition susceptibility $\tilde{\chi}^{(1)}$ results in first order Raman scattering (Cardona and Güntherodt 1982).

Classically an excitation (denoted by m) may be treated as a plane

wave characterized by a frequency ω, a wave vector $\mathbf{q}$ and a collective excitation coordinate amplitude $Q_m(\mathbf{q},\omega)$ which has the transformation properties of the crystal point group at $\mathbf{q}$. In the case of optical phonons, Q_m correspond to the amplitudes of the normal modes $U_m(\mathbf{q},\omega)$. Then $\tilde{\chi}^{(1)}$ may be written as

$$\tilde{\chi}^{(1)}_{\alpha\beta} = \sum_m (R_m)_{\alpha\beta} Q_m \qquad (2.29)$$

where (R_m) are known as the first-order Raman tensors associated with the excitations Q_m.

Applying group theory to $\tilde{\chi}^{(1)}_{\alpha\beta} = \sum_m (R_m)_{\alpha\beta} Q_m \neq 0$ which is a requirement for the allowed first order Raman scattering, the condition for an allowed scattering is obtained as (Pinczuk and Burstein 1975): the irreducible representation $\Gamma_{\alpha\beta}$ which describes the symmetry properties of $\alpha\beta$ component of a second rank tensor and the irreducible representation of the crystal point group which describes the symmetry of the phonon wave functions Γ_l must satisfy the following

$$\Gamma_l \times \Gamma_{\alpha\beta} \supset \Gamma_1 (=A_1) \qquad (2.30)$$

Where Γ_1 $(=A_1)$ is the totally symmetric representation of the point group of the crystal.

With Eq.(2.30), the selection rules of Raman scattering can be deduced. In a crystal with inversion symmetry $\Gamma_{\alpha\beta}$ has even parity while Γ_l, for $q \approx 0$ optical phonons may have even or odd parity depending on the crystal structure and on the phonon being considered (Pinczuk and

Burstein 1975). From Eq.(2.30) it follows that, in crystals with inversion symmetry, such as CuO, only phonons with even parity (g modes) are Raman active.

The infrared selection rules may also be obtained by considering the structure of the crystal in another, but in principal, similar way (Heine 1960). For a crystal structure such as CuO with inversion symmetry, it has been found (see Brüesch 1986 for details) that g modes which have even parity are Raman active and infrared silent, while u modes, with odd parity, are infrared active but Raman inactive.

So from Eq.(2.22), we have, for a CuO crystal, three acoustic modes A_u+2B_u, three Raman active modes A_g+2B_g, and six infrared active modes $3A_u+3B_u$. Loudon (1964) calculated the forms of Raman tensors of various point groups by considering the symmetries of elements in expressions like Eq.(2.23). For point group C_{2h}, he showed that the forms of Raman tensors of the active Raman phonons A_g (Γ_1^+) and B_g (Γ_2^+) modes are

$$R_{A_g} = \begin{pmatrix} a & & d \\ & b & \\ d & & c \end{pmatrix} \tag{2.31}$$

$$R_{B_g} = \begin{pmatrix} & e & \\ e & & f \\ & f & \end{pmatrix} \tag{2.32}$$

With Eq.(2.27), the condition for Raman scattering can be written as

$$\hat{e}_s \cdot \tilde{\chi} \cdot \hat{e}_i \neq 0 \tag{2.33}$$

which determines a set of selection rules for various directions of the polarizations of the incident and scattered light $\hat{e}_i$ and $\hat{e}_s$. With Eq.(2.29) we have

$$\sum_m [\hat{e}_s \cdot (R_m)_{\alpha\beta} \cdot \hat{e}_i] \, Q_m \neq 0 \tag{2.34}$$

thus one can see, for example, only scattering from the A_g mode can be observed when $\hat{e}_s = \hat{x}$ and $\hat{e}_i = \hat{x}$ since $(R_{A_g})_{xx} \neq 0$ but $(R_{B_g})_{xx} = 0$.

3. EXPERIMENTAL

1) Samples

The CuO crystals investigated in this work were obtained from three sources. One set of crystals was grown by vapor transport with hydrogen chloride as a transport agent by Dr. Wold's group in the Department of Chemistry at Brown University (Desisto et al. 1989). Another crystal was grown by a flux method (Wanklyn and Garrard 1983) and was provided by Dr. Wanklyn of the Clarendon Laboratory at University of Oxford. The remaining crystals were grown by Mr. Per Joensen of the SFU physics department using the same flux method, with starting composition and growth temperatures identical to those described by Wanklyn and Garrard (1983). 15g of CuO, 4.5g V_2O_5, 5.4g MoO_3 and 3.4g K_2CO_3 were used as the starting materials. The mixture was placed inside a platinum crucible and heated to 1100°C, it was then cooled with a cooling rate of 6°C/hour. At 910°C the crucible was removed from the furnace and rapidly inverted while the flux was still liquid, the crystals remained attached at the crucible base. The size of a typical crystal obtained was about $10\times3\times2mm^3$. Most of the Raman spectra were collected from two of these crystals, one grown by vapor transport (sample S1) and one grown at SFU by the flux method (sample S2). Spectra obtained from the Oxford sample were very similar to those obtained from sample S2.

The Raman spectra of CuO were acquired from the as grown surfaces of crystals without polishing. Sample S1 had a cleavage surface with some tiny but visible layer structures. The surface was found by Laue and conventional X-ray diffraction (Figs.3.1 and 3.2) to be approximately parallel to the a-b plane, and the a- and b-directions of this surface were also determined. Sample S2 had a relatively rough and slightly concave surface with metallic luster, the Laue pattern was relatively poorer, the surface was found to be parallel to the [110] plane. Both surfaces were carefully cleaned with acetone and ethanol before measurements. The best (clean and flat) regions of samples were selected to acquire spectra by observing the enlarged images of crystals on the slit plane of the spectrometers.

The CuO crystals were also investigated after annealing at 500^{o}C in flowing oxygen for 24 hours. The purpose of the annealing was to compensate escaped oxygen atoms and reconstruct the crystals. The crystals were placed on a ceramic boat and loaded into a glass pipe in a horizontal furnace, below 460^{o}C the increasing and decreasing rates of temperatures were about 2^{o}C/min, in the range of 460^{o}C-500^{o}C the rates were reduced to 1^{o}C/min. The flux of oxygen was kept to be about 60 cm^{3}/min. Raman measurements were obtained both before and after the annealing. The spectra obtained were very similar except a slight increase of the peak intensities in sample S1, implying that samples

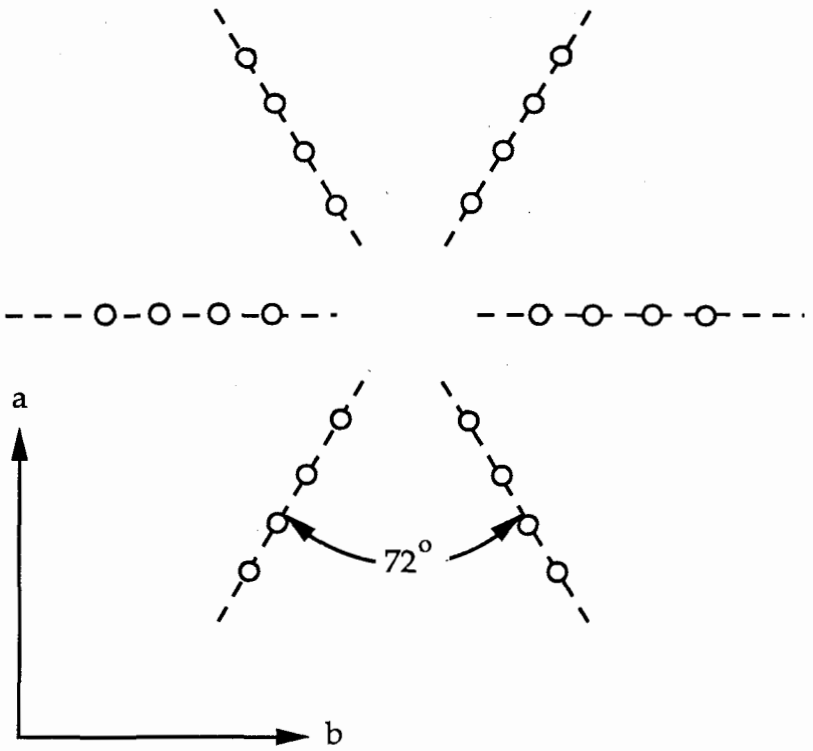

(a)

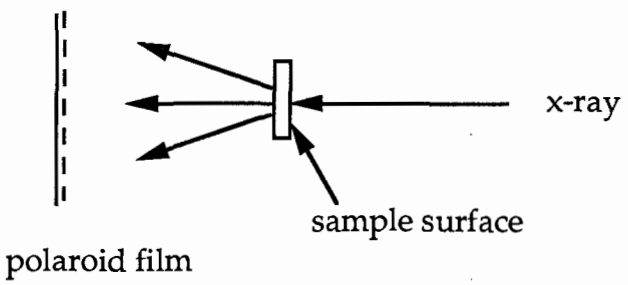

(b)

Fig.3.1 The schematic Laue pattern of the crystal S1(a) (reproduced from the original photograph), and the scattering geometry(b). The observed x-ray spots fall in the dashed lines as indicated schematically in the figure. The angle 72° is just the angle between [110] and $[\bar{1}10]$ ribbons, indicating that the surface is approximately perpendicular to the [001] axis.

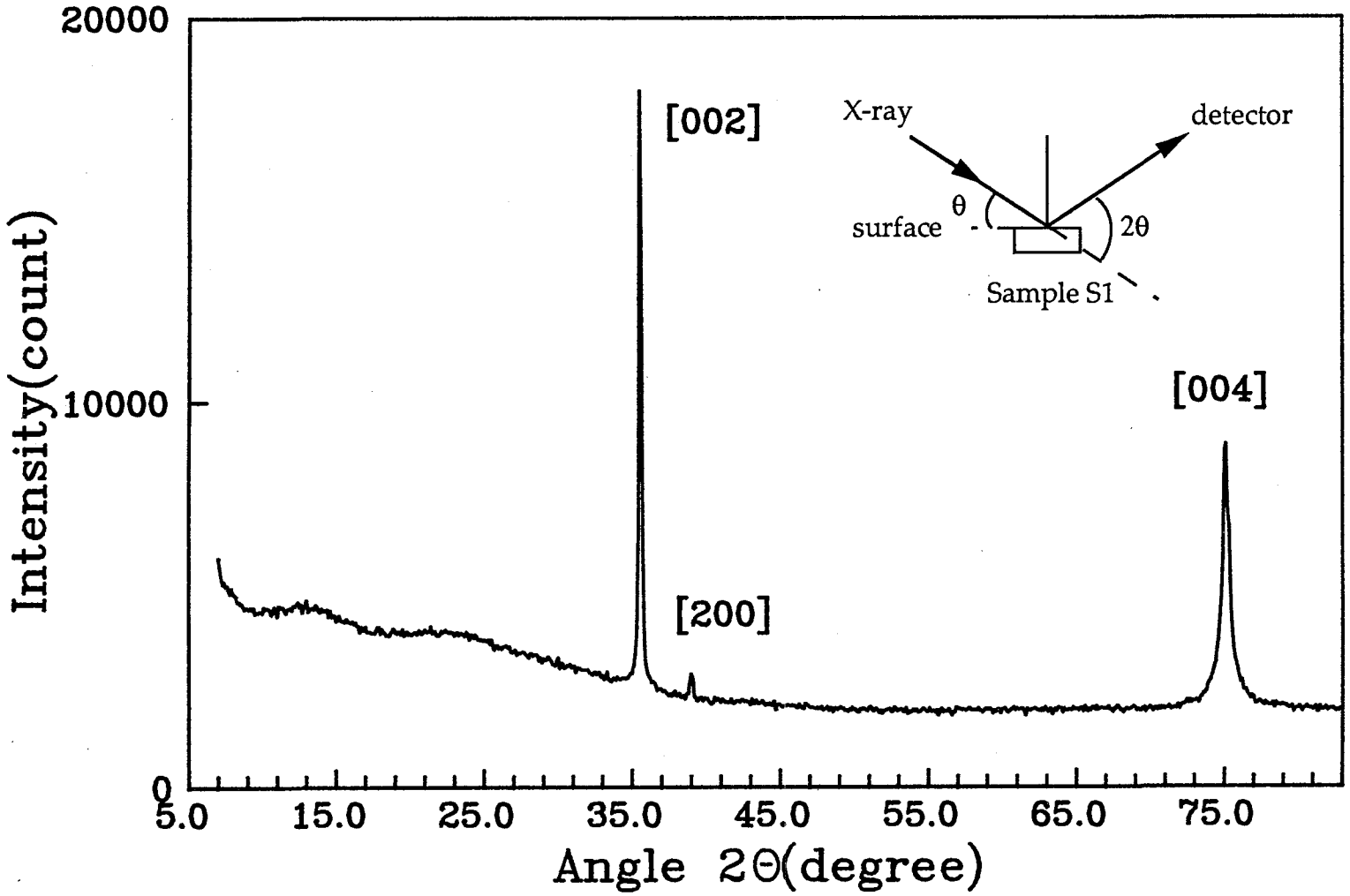

Fig. 3.2 The X-ray diffraction intensity of the CuO crystal S1. The scattering geometry is also shown. Two strong peaks from [002] and [004] layers are observed, indicating that the surface is approximately perpendicular to the [001] direction.

under investigation were quite stable.

Isotopic $Cu^{18}O$ powder was obtained from MSD Isotopes, a division of Merck Frosst Canada Inc.. The samples studied were obtained by pressing powders into small pellets with a pressure of 14K bar. The purity of the sample was 99.3%. To avoid ^{16}O contamination the pellets were not sintered, so they were relatively loosely packed and the surfaces were not as good as those of CuO crystals.

2) Experimental apparatus

Raman scattering experiments were carried out on both a double and a triple grating spectrometers (Fig.3.3). The samples were excited by Argon ion lasers with either the 488.0 or 514.5nm lines. The incident power was measured at the sample and usually it was set to be 50mW. The laser was focused onto the sample with a cylindrical lens, the laser spot was about $0.1\times5mm^2$, so the light intensity was about $10W/cm^2$. The sample was glued on a small piece of copper disc with commercial nail polish, and the disc was then mounted onto the cold finger of an Air Products' displex refrigerator in which the temperature of the sample could be varied from 15 to 300K. To enhance the heat conductivity between copper disc and cold finger some vacuum grease was added between them. The temperature increase due to local heating of the samples by the incident laser light was estimated to be 20±10K from a Stokes

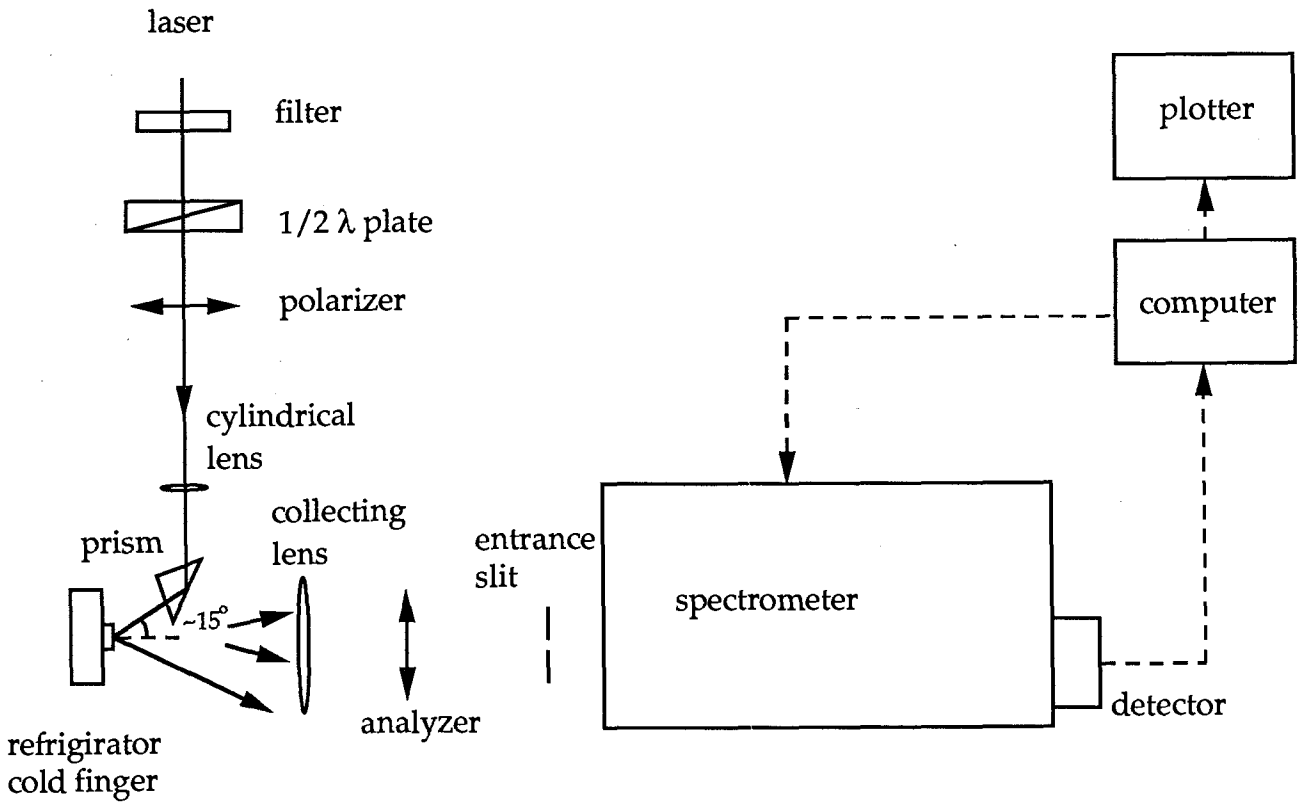

Fig. 3.3 Experimental setup.

anti-Stokes measurement (Chrzanowski and Irwin 1989).

The sample surfaces from which the spectra were collected were all arranged to be perpendicular to the detected scattered light. To avoid reflected light from entering spectrometer directly, the laser beam focused onto sample was tilted by about 15°-20° as shown in Fig.3.3 and 3.4. The scattered light from the copper substrate was reduced by using an aperture to reduce the line-like image on the sample to a length shorter than the width of the sample.

Both the double and triple spectrometers used were controlled by IBM/PC computers. The scattered photons from the scanning double grating spectrometer were detected by a cooled Hamamatsu R943-02 photomultiplier tube. The scattered light dispersed in the triple spectrometer was detected with an ITT Mepsicron imaging detector. Output signals were interfaced to PCs and were plotted after storing and processing (Fig. 3.3). Sometimes, in acquiring spectra with the double spectrometer, the measured signals were very weak and the measurement had to be repeated a few times, and the final spectrum was obtained by summing all these independent measurements. Typically, when the measurements were conducted with the double grating spectrometer, the total time used for collecting a data point was about 10 seconds and a full spectrum covering frequency region of 100-6000cm^{-1} required more than 16 hours. However it took only about 30 minutes to obtain a spectrum on the triple

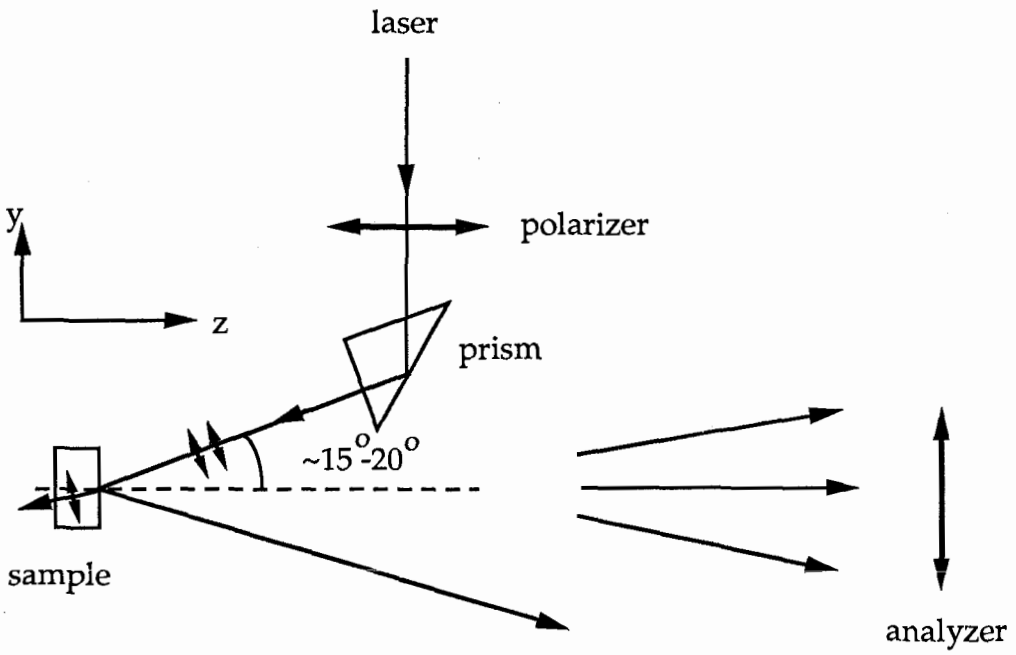

Fig. 3.4 Scattering geometry showing the incident light is polarized in the horizontal(yz) plane.

spectrometer covering the range 500 to 3000cm^{-1}.

The resolution of a spectrometer depends mainly on the slit width of the spectrometer. In this work the slits were usually adjusted so that the resolution was about 3-5cm^{-1}, a little narrower than the width of a typical phonon Raman peak (5-10cm^{-1}) (Hathaway 1971). As some scans were conducted over spectral regions as large as 6000cm^{-1}, the response of spectrometers had to be calibrated. The spectrum of a standard lamp (providing radiation equivalent to that of a black body at 3000K) was measured to calibrate the spectrometer systems. However, as we can see from Fig.3.5(a), in the frequency region below 2600 cm^{-1}, which covers all the interesting features, the response of the triple spectrometer is approximately a constant (dashed line in Fig.3.5(a)), and the spectra obtained using the triple spectrometer are thus shown without modification. Spectra collected from the double spectrometer and extend beyond 1200cm^{-1} were calibrated according to Fig.3.5(b).

3) Scattering configurations

The Raman scattering configuration can be used to identify the symmetry properties of phonons. If the incident light propagates along the $\bar{z}$ direction of the crystal with polarization in the x direction, and the scattered light propagates along z with y polarization being selected, the scattering configuration is designated $\bar{Z}(XY)Z$. As is

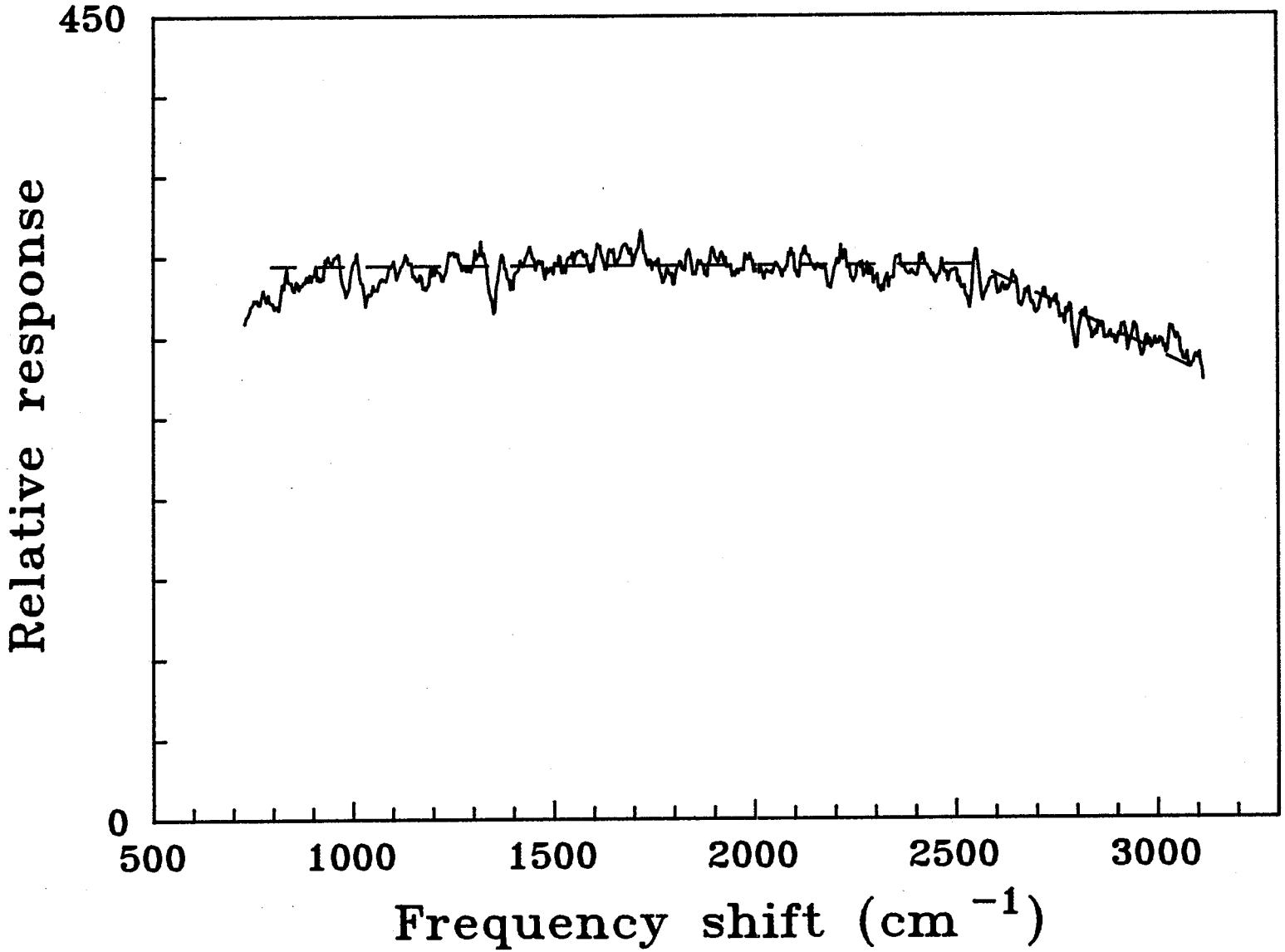

Fig. 3.5(a) The non-normalized response of the triple grating spectrometer. The dashed curve is an experimental fit, it consists two straight lines. In the frequency region 700-2600cm^{-1} the slope=0

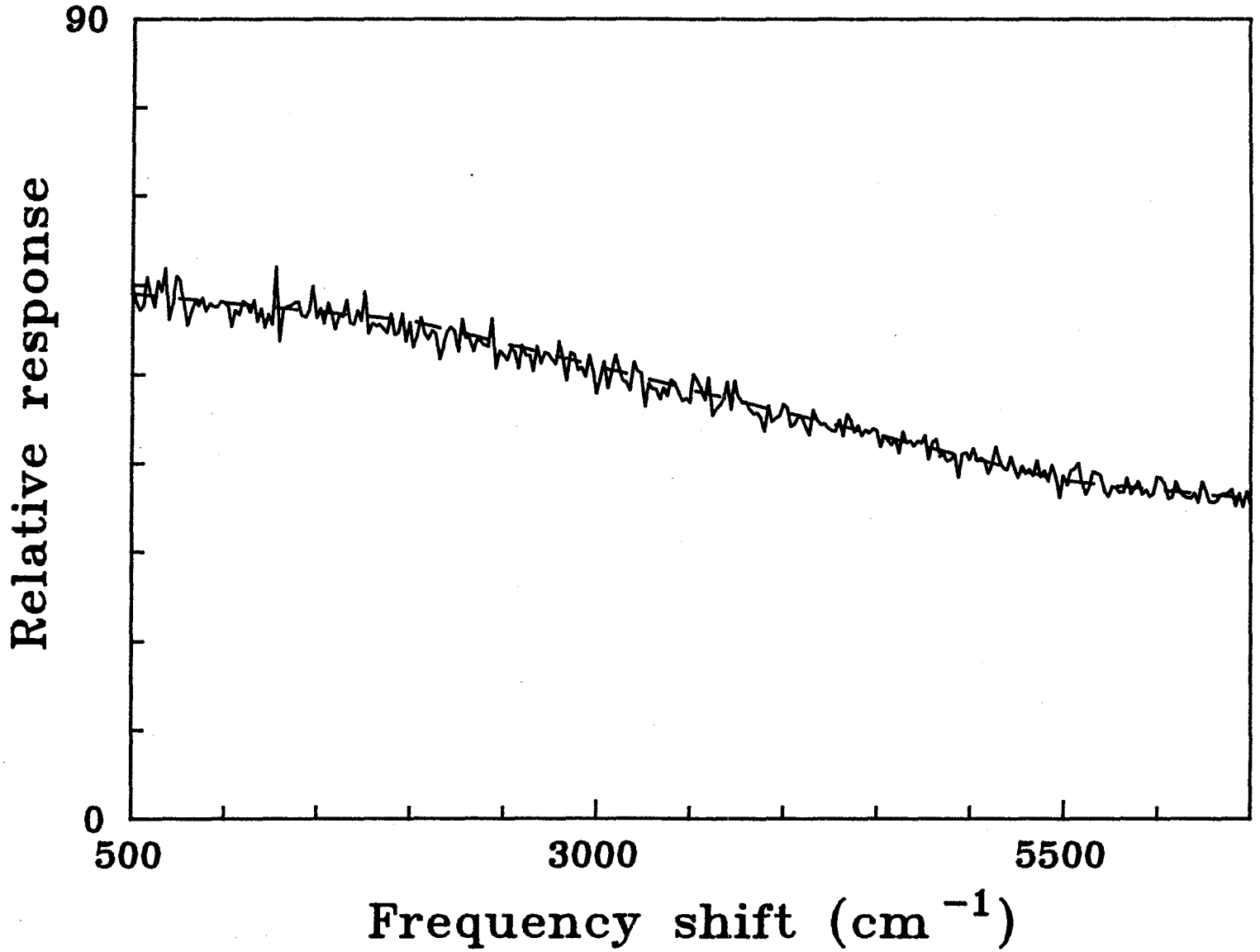

Fig. 3.5(b) The non-normalized response of the double grating spectrometer. The dashed curve is an experimental fit, it consists of three inclined lines.

discussed in Chapter 2.6, the scattering of a particular excitation is observed, for example, in the (XY) configuration only when matrix element of Raman tensor $(R_{yx})_m \neq 0$. Therefore from the forms of Raman tensors of A_g and B_g modes (Eq.(2.31) and (2.32)), we expect that the A_g mode of CuO may be observed in the (XX), (YY), (ZZ) and (XZ) configurations, while in the (XY) and (YZ) configurations only the B_g modes should be observed.

One should note however that in birefringent materials depolarization due to birefringence may affect the measured results when the incident or scattered light is not polarized along one of the optic axes x', y' and z' (Berenblut et al. 1971). In the monoclinic CuO crystals the y-axis coincides with the y' optic axis, and the x' and z' axes lie in the a-c plane (Berenblut et al. 1971). We assume that they are approximately parallel to x and z axes, respectively. This may be a reasonable assumption since $\beta=99.54^{\circ}$ is fairly close to 90°. The depolarization may also be small if the birefringence in CuO is small. But in any event, depolarization can be minimized by using polarizations along the y-axis to the greatest extent possible.

Sample S1 provided an optimum crystal orientation for observation of polarized spectra in that the large face of the crystal was almost perpendicular to the z-axis. The polarizations of incident and scattered light could then be aligned along the y-axis and birefringent effects

thus minimized. In our polarized measurements the crystal was oriented such that the z axis of the crystal was normal to the slit plane of the spectrometer, and the y and x axes were set to be parallel to the vertical and horizontal directions, respectively (see Fig.3.4).

All scattering experiments were performed with incident light propagating in a plane parallel to the xz plane of the crystal and polarized horizontally (that is, in the xz plane) or vertically (along the y direction). The scattered light propagated along the z-direction and the polarization in the x or y directions were selected (Fig.3.4). With incident light being vertically polarized, only the y-component is present in the incoming light, the spectra for (YX) and (YY) scattering geometries are obtained. But when the incident light is polarized in the horizontal (xz) plane both x and z components are present. Thus with the scattered light being polarized along the y and x axes, spectra obtained are of (XY) plus (ZY) and (XX) plus (ZX) scattering configurations, respectively. However, since the direction of the incident light propagated inside the crystal would be less than 15° from the z axis if the index of refraction CuO is larger than one, we expect that the major contributions come from (XY) and (XX) configurations.

4. RESULTS AND DISCUSSIONS

The spectra shown in Fig.4.1-4.3 and 4.5-4.8 were obtained with either the 514.5nm or the 488.0nm lines of Ar ion lasers. It should be noted, however both lines and both spectrometers were used to measure every spectrum, it was found that all spectra taken in equivalent geometries were very similar, with only small changes in the relative intensity in some cases. In some measurements, the signal-to-noise ratio was very poor even after a number of scans, and the final spectrum was obtained by summing several independent measurements until an acceptable ratio was achieved.

1) One-phonon scattering

Fig.4.1 shows the Raman spectra of CuO crystals in the frequency region between 100 and 800cm^{-1}, obtained with the sample at temperatures of 15 and 300K. It can be seen that there are three strong peaks at 298, 344 and 632cm^{-1} at 300K. At 15K they shift to 303, 350 and 636cm^{-1} and become slightly sharper. These three peaks were observed in spectra obtained from a CuO powder pellet by Chrzanowski and Irwin (1989). The temperature dependence of the frequencies is quite typical in that the increase in frequency can be approximately accounted for by the contraction of the lattice, as the temperature is lowered (Sherwood 1972). These three peaks were assigned to the A_{1g} (298cm^{-1}), B_{1g}

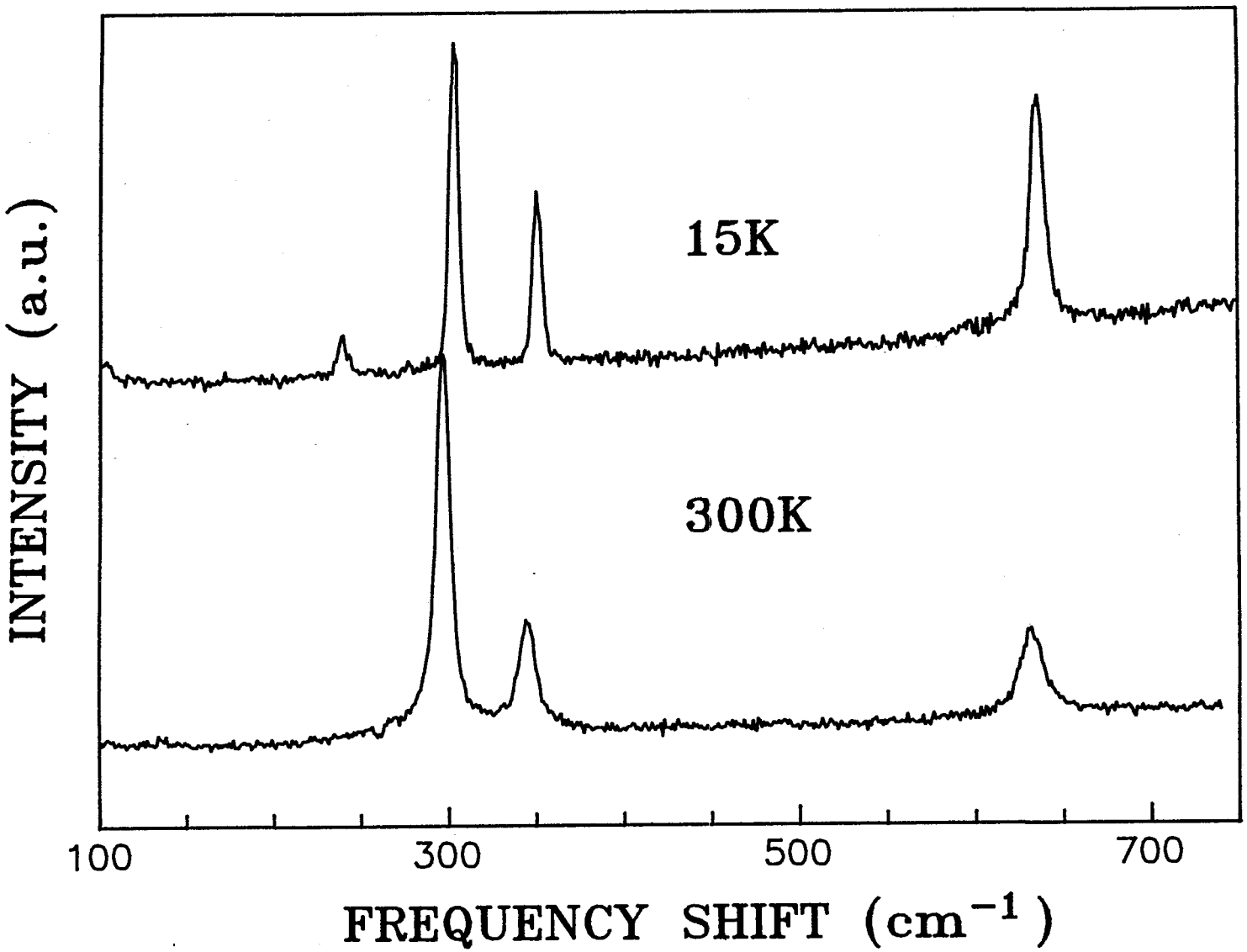

Fig.4.1 The Raman spectrum of CuO for 15K and 300K. Excited by the 514.5nm line of an Argon ion laser and collected from the triple grating spectrometer.

($344cm^{-1}$) and B_{2g} ($632cm^{-1}$) phonons of CuO by Chrzanowski and Irwin on the basis of depolarization ratios in spectra obtained from pressed and sintered pellets.

Polarized spectra obtained from single crystals must be used however to obtain an unambiguous assignment. Fig.4.2 and 4.3 are spectra from crystal S1 at 300K with the incident light polarized in the y direction (the b axis of the crystal) and in the xz (ac) plane, respectively. The experimental deviation of polarization directions from crystal axes was estimated to be less than $\pm 5^{o}$ (Chapter 3.3). Only the $298cm^{-1}$ mode is observed in the (YY) and (XX)+(ZX) configurations, in the (XY)+(ZY) and (YX) configurations the 346 and $632cm^{-1}$ modes are present while the $298cm^{-1}$ mode is suppressed.

As already discussed in Chapter 2.6, the xx, yy zz and xz elements of the first order Raman tensor B_g are equal to zero (Eq.2.28) and the xy and zy elements are nonzero. For the A_g mode, it is the opposite (Eq.2.27). Thus in the (XX), (YY) (ZZ) and (ZX) configurations the A_g mode should be observed and the B_g modes should be absent. On the other hand the xy, yx and yz elements of the B_g tensor are nonzero but that of the A_g tensor are zero, so only the B_g modes should be observed in the (YX), (XY) and (ZY) configurations. Thus spectra Fig.4.2 and 4.3 are completely consistent with all predictions if the $298cm^{-1}$ peak is considered as an A_g mode and the two others as B_g modes. These

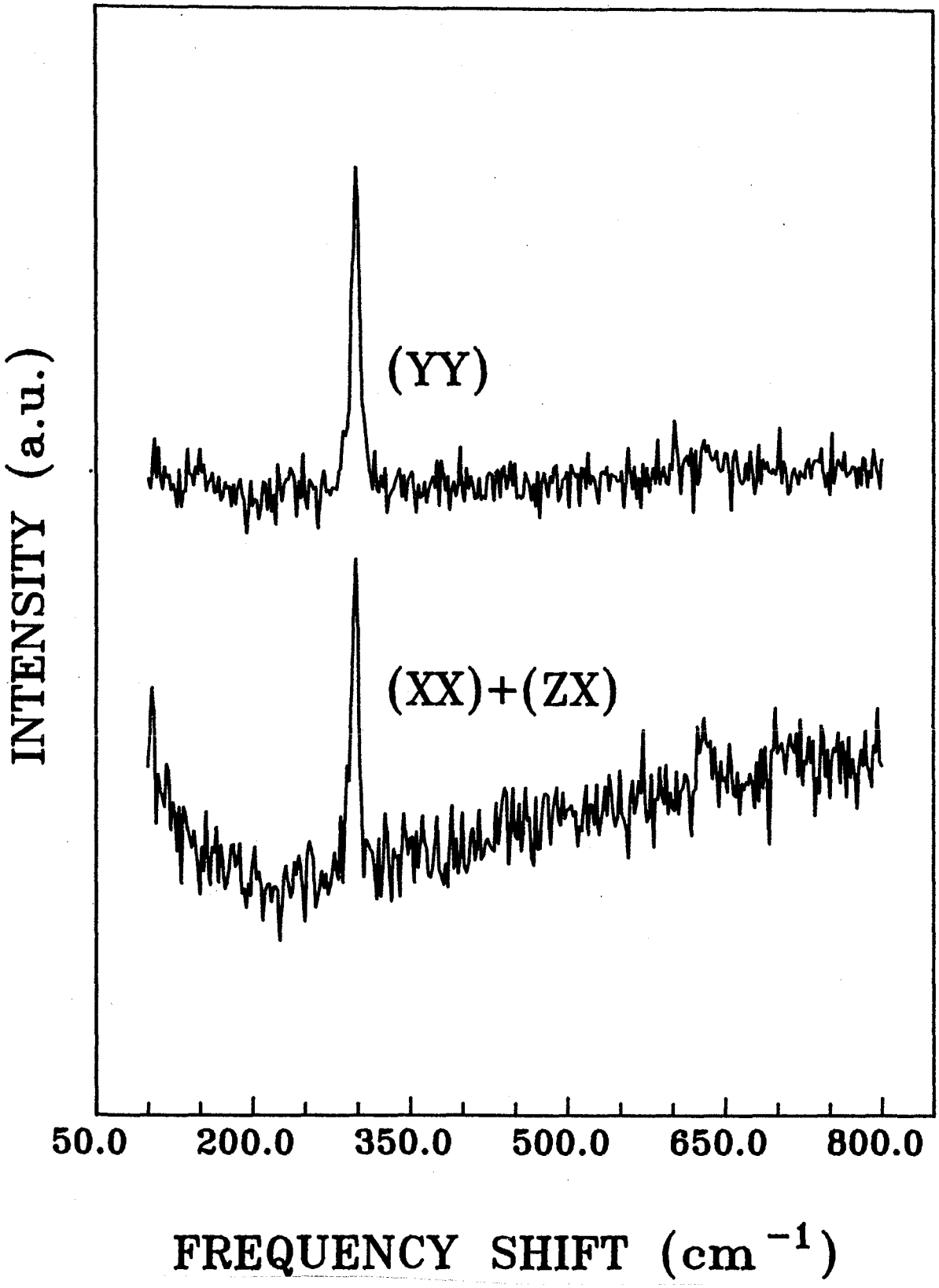

Fig.4.2 Room temperature first-order Raman spectra of CuO in the (YY) and (XX)+(ZX) polarization geometries.

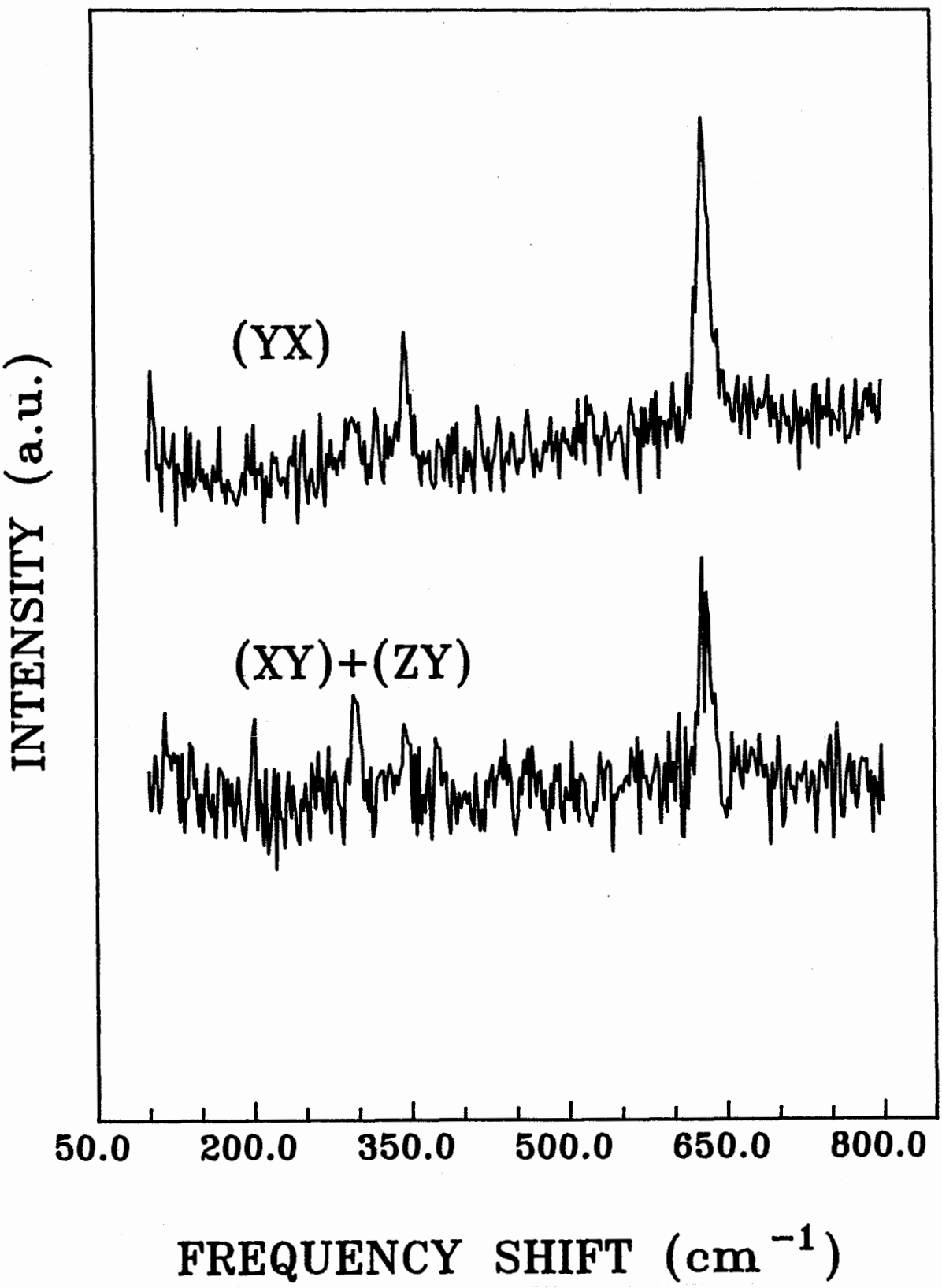

Fig.4.3 Room temperature first-order Raman spectra of CuO in the (YX) and (XY)+(ZY) polarization geometries.

frequencies increase as temperatures are lowered, which is typical of phonon scattering, so we can unambiguously assign the 298cm^{-1} peak to an A_g mode, and assign the features at 346cm^{-1} and 632cm^{-1} to the first order scattering from the expected B_g modes.

Experiments with the incident power unchanged showed that the Raman signals of the (XX)+(ZX) and (XY)+(ZY) geometries obtained with the incident light polarized in the xz plane were very weak compared with signals of the (YX) and (YY) geometries in which incident light was polarized in the y-direction, and it took several measurements to obtain the present (XX)+(ZX) and (XY)+(ZY) spectra. Recently, Goldstein et al. (1990) found that the A_g mode was strongly polarized along one of the crystal axes which could be an a or b axis. If this axis is the b axis, their result is consistent with our observations.

2) Force constants and normal modes

From the above, we conclude that $\omega(A_g)$=298cm^{-1}, $\omega(B_{1g})$=346cm^{-1} and $\omega(B_{1g})$=632cm^{-1} at room temperature. However, we need additional frequencies to determine the force constants of the VFF model (Chapter 2.3). The frequencies of six infrared modes have been obtained from neutron scattering (Reichardt et al. 1990) and infrared experiments (Guha et al. 1990, and see references in Hagemann et al. 1990). They are listed in Table 4.1, where the frequencies taken from the neutron

scattering curves are those of the transverse optic modes. These modes should not be affected by any long range Coulomb interactions which are not included in our VFF model (Chapter 2.3). One can see from the table that there are some discrepancies in the observed infrared data, and in most cases the symmetries of phonons are not known. The only complete set of data for odd modes with a clear symmetry assignment was obtained by Reichardt et al. (1990) from neutron scattering. Reichardt et al.. determined the phonon dispersion of CuO in detail and their netron results for the Raman active phonons are in good agreement with our results. The infrared data obtained by Guha et al. (1990) from infrared reflectance experiments are relatively close to the neutron data, although we can still see some big differences. This is especially true for the frequency of B_{3u} mode, the deviation of which is about $70cm^{-1}$. Further measurement is needed to obtain more accurate data. Since only the neutron data provided a complete set of frequencies for the infrared active TO modes, these values have been used to determined the force constants. Together with Raman frequencies these TO phonon frequencies are listed in Table 4.2.

6 stretching and 5 bending force constants defined in Chapter 2.3 have been introduced into the Valence Force Field (VFF) model to construct the dynamical matrix M (Eq.2.14).

Table 4.1 Observed infrared data at room temperature.

	observed frequencies (cm^{-1})	references
A_u	164, 355	
B_u	147, 480, 603	Guha et al. (1990)
A_u	164, 330, 423	
B_u	146, 480, 530	Reichardt et al. (1990)
	148, 163, 323, 446, 481, 598	Popovic et al. (1988) and Degiorgi et al. (1988)
	484, 534, 582	Zhao et al. (1987)
	[a] 69w, 106m,br, 128sh, 147s, 164s, 320sh, 400m, 480s, 510vs, 580sh	Hanuza et al. (1988)
	452, 483, 542, 583	Hageman et al. (1990)
	410, 500, 610	McDevitt and Baun (1964)

a) w=weak, m=medium, s=strong, vs=very strong, sh=shoulder, br=broad.

Table 4.2 Observed and calculated frequencies for CuO and $Cu^{18}O$ (in cm^{-1}).

	CuO			$Cu^{18}O$	
mode	obs(15K)	obs(300K)	cal	obs(300K)	cal
Raman mode					
A_g	303	298	298	282	281
B_{1g}	350	346	346	328	327
B_{2g}	636	632	632	596	596
IR mode[(a)]					
A_{1u}		164	164		162
A_{2u}		330	330		329
A_{3u}		423	423		410
B_{1u}		146	146		145
B_{2u}		480	480		460
B_{3u}		530	530		506

a) The observed infrared frequencies for CuO are from neutron scattering experiment (Reichardt et al. 1990).

By diagonalizing the matrix M, eigenvalues ω_j^2 and eigenvectors U_j can be calculated. Since ω_j^2 and U_j are functions of force constants k_i, matching of the calculated ω_j with observed values may be obtained when a proper set of k_i is chosen. A computer FORTRAN program with a subprogram for diagonalizing M was used for this fitting. In the program force constants were adjusted step by step until the least-square-error was reduced to the desired value (least square error method).

We expected that the stretch force constants of the shorter bonds and the bending constants of the smaller angles would be relatively large, and thus only k_1, k_2, k_3 and k_4 were taken into account initially (that is, the remainding k_i were set to be zero). The initial values of k_1 (1.95Å) and k_2 (1.96Å) were chosen to be 152 and 149Nm^{-1}, that used for the Cu-O bonds of 1.95Å and 1.96Å in $YBa_2Cu_3O_6$ and $YBa_2Cu_3O_7$ in lattice dynamical calculations carried out by Bates (1989), and k_3 and k_7 were initially assumed to be close to zero (~1Nm^{-1}). The resulting k_1 and k_2 were about 70Nm^{-1}, only about one half of the initial values. With only these 4 force constants a very poor fit was obtained. The minimum value of the square-root-error, defined as $(\sum_{i=1}^{12} (\omega_i^{th}-\omega_i^{exp})^2)^{-1/2}$, that could be obtained was about 200cm^{-1}. As additional force constants were considered, however, an almost exact fit was obtained. The final results for k_i, with a square-root-error $(\sum_{i=1}^{12} (\omega_i^{th}-\omega_i^{exp})^2)^{-1/2}$ of less than 0.1cm^{-1}, are shown in Table 4.3.

Table 4.3. Calculated force constants for CuO.

force constant	bond type	distance(Å) or angle	cal. value[a] ($k_i r_1 r_2$[b]) of this work	results of F-G method[c]	results of ion model[d]
k_1	O3-Cu1	1.9608	62.4	75.0	142.2
k_2	O3-Cu1"	1.9509	69.8	73.4	146.7
k_3	Cu1-O3-Cu1"	95.72°	20.5 (78.1)	(60.0)	
k_4	Cu1"-O3-Cu2	104.03°	4.5 (17.3)	(10.0)	
k_5	Cu1-O3-Cu2	145.82°	0.5 (2.0)	(0.3)	
k_6	Cu1"-O3-Cu2'	108.85°	4.0 (15.0)	(9.0)	
k_7	O3-Cu1-Cu4[b]	84.28°	23.7 (90.4)	(70.0)	
k_8	Cu1-Cu2'	3.0830	25.0	30.0	10.9
k_9	Cu1"-Cu2'	3.1734	36.7	27.5	30.7
k_{10}	O3-O4	2.6246	20.1	7.0	25.5
k_{11}	Cu1-Cu2	3.7484	2.3	16.7	

a) Force constant units are: stretching, Nm^{-1} and bending $Nm^{-1}rad^{-2}$.

b) For bending force constants only, unit is: $10^{-20}Nm\ rad^{-2}$.

c) Guha et al. (1990). Units are the same as (a) and (b).

d) Reichardt et al. (1990). Only longitudinal force constants $F=d^2\Phi/d^2r$ are shown, unit is Nm^{-1}.

Since we had less force constants (11) than frequencies to be fitted (12) (The frequencies of three acoustic modes were zero at Γ point and they were not listed in Table 2.2), the choice of k_i were not unique. When a different set of initial values was introduced, the resultant k_i obtained were slightly different from those shown in Table 4.3. To examine the VFF model, a series of very different initial values were introduced to calculate force constants k_i. It was found by comparison that the difference between any two sets of k_i was relatively small ($\sum_{i=1}^{11} |k_i^{th1} - k_i^{th2}| < 30 Nm^{-1}$). We also found that, the relative magnitudes of the 6 stretch force constants remained unchanged no matter what initial values were introduced, as did the relative magnitudes of the 5 bending force constants. Secondly, while the variations of the five small force constants k_4 to k_6, k_{10} and k_{11} were relatively large, the changes of the six larger constants, k_1, k_2, k_3, k_7, k_8 and k_9, were less than ±10%. Furthermore, one can see from Table 4.3, the bending force constants increase as the angles decrease. If the anomalously large k_9 (Cu-Cu bond of 3.0830Å) and k_{10} of O-O bond are excluded, stretch force constants also increase as bond lengths decrease. For a large enough angle like ψ_5=145.82° and long bond like r_{11}=3.7484Å, the force constants (k_5 and k_{11}) are almost zero. These are in agreement with the theoretical expectations.

The eigenvectors of various modes at **k**=0 have also been calculated using the eigenvalues (ω_i^2) presented in Table 4.3. The resultant atomic

Table 4.4 Normalized displacements of phonon modes for CuO.

Also given are frequencies of phonons.

MODE		A_g	B_{1g}	B_{2g}	A_{1u}	A_{2u}	A_{3u}	B_{1u}	B_{2u}	B_{3u}
$\omega(cm^{-1})$		298	346	632	164	330	423	146	480	530
	x	-	-	-	-.69	.13	-.20	.08	-.13	-.11
Cu1	y	-	-	-	-.16	-.10	.17	.60	.12	.02
	z	-	-	-	-.01	-.69	-.15	.05	-.11	.13
	x	-	-	-	.69	-.13	.20	.08	-.13	-.11
Cu2	y	-	-	-	-.16	-.10	.17	-.60	-.12	-.02
	z	-	-	-	.01	.69	.15	.05	-.11	.13
	x	-	-.70	.14	-	-	-	-.32	.51	.43
O3	y	.71	-	-	.64	.37	-.68	-	-	-
	z	-	-.14	-.70	-	-	-	-.17	.44	-.53
	x	-	.70	-.14	-	-	-	-.32	.51	.43
O4	y	-.71	-	-	.64	.37	-.68	-	-	-
	z	-	.14	.70	-	-	-	-.17	.44	-.53

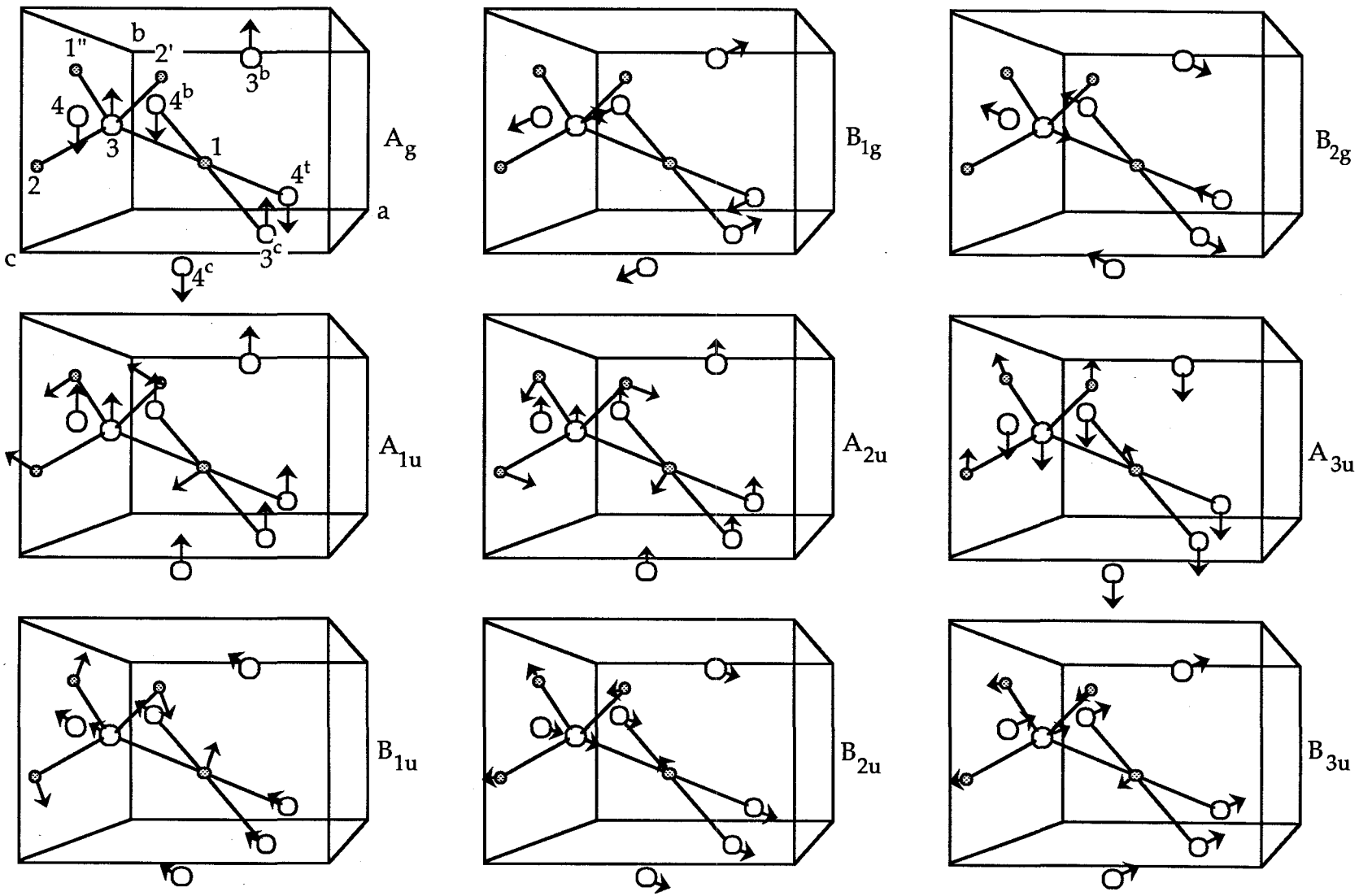

Fig. 4.4 The schematic atomic displacements of CuO. Labels of atoms are the same as that in Fig.2.1.

displacements for the vibrational modes are listed in Table 4.4 and shown diagrammatically in Fig.4.4. As is evident from these results the A_g and B_g modes involve motion of the oxygen atoms only with displacements in the b-direction for A_g and perpendicular to the b-axis for B_g modes. The infrared active, or odd, modes involve motions of both the Cu and O atoms with the induced dipole in the b-axis direction for the A_u modes and perpendicular to b for the B_u modes.

According to Herzberg (1950), when one type of atom is replaced by an isotopic atom, it can be assumed that the potential energy function and configuration of the crystal are changed by negligible amounts, and thus the vibrational frequencies are altered only by the change in mass. The room temperature Raman measurement of cupric oxide powder formed with isotopic ^{18}O atoms was performed and the result is shown in Fig.4.5. The spectrum of a normal CuO powder pellet at room temperature is also shown in the figure. No CuO phonon peaks were observed in the $Cu^{18}O$ spectrum indicating that the $Cu^{18}O$ samples were pure, that is, not contaminated by CuO. As can be seen from Fig.4.5 the three peaks that occur at 298, 345 and 632 cm^{-1} in CuO are all shifted to lower frequencies in the $Cu^{18}O$ spectrum. In the room temperature $Cu^{18}O$ spectrum these three peaks occur at 282 (A_g), 328 (B_g) and 596 (B_g)cm^{-1}. Using the force constants obtained from the calculation of the CuO vibration frequencies, the VFF model has been used to calculate the frequencies of $Cu^{18}O$ by merely changing the mass of the oxygen atom. The

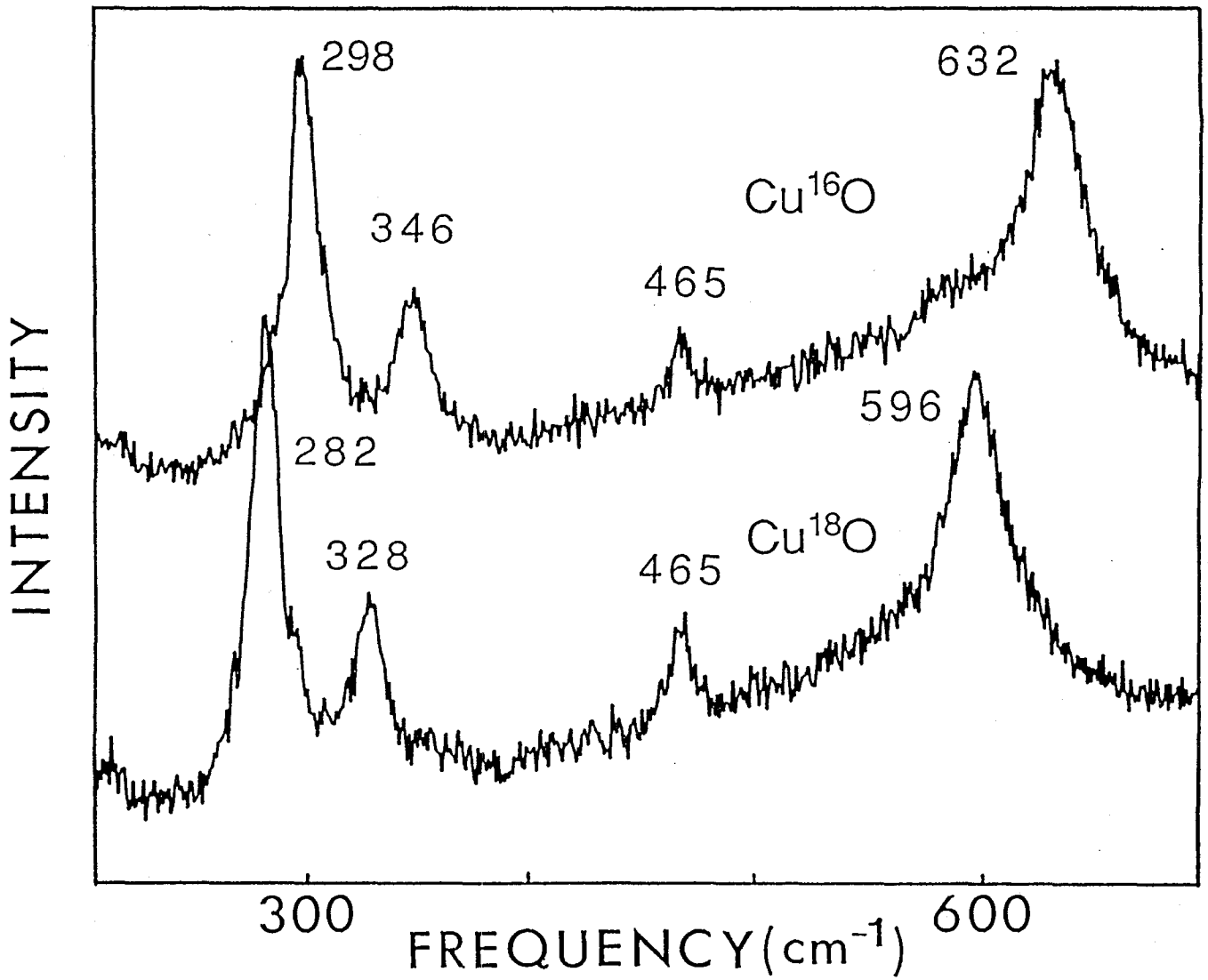

Fig.4.5 Room temperature Raman spectra of CuO (upper trace) and $Cu^{18}O$ (Lower trace) showing the thrre Raman active phonons and the feature at 465cm^{-1}. The two spectra are vertically displaced for clarity.

results are listed in Table 4.2 and they are in excellent agreement with the experimental results. This agreement indicates that the force constants used in the model reliably represent the non-Coulomb interatomic forces in the crystal. The excellent agreement between the calculated and measured isotopic frequency shifts also lends confidence to the eigenvectors calculated from the VFF model.

Guha et al. (1990) have independently calculated the force constants of CuO with Wilson's F-G method (Wilson et al. 1955). The 11 force constants used here are among the 12 used in their work. They have chosen somewhat different IR frequencies for the determination of their parameters. However, they arrived at similar vibrational modes, and most of their force constants were quite close to the results obtained in this work except for the relative magnitudes of k_8 and k_9 (Table 4.3).

Reichardt et al. (1990) have recently measured the phonon dispersion curves in CuO using neutron scattering. They have used a 21-parameter rigid ion model in an attempt to reproduce the measured dispersion curves. This model thus included long range Coulomb interactions and to obtain reasonable agreement they assumed an effective charge of 0.82. In general, at $\mathbf{k}=0$, their relative magnitudes of the stretch force constants between the given atomic pairs are consistent with our results (Table 4.3), in particular, the relative magnitudes of k_8 and k_9. This is possibly because their TO frequencies

were used in determining our force constants.

Another basis for comparison is provided by the lattice dynamics calculations which have been carried out (Bates 1989) on the superconducting cuprates $YBa_2Cu_3O_7$ and its non-superconducting parent $YBa_2Cu_3O_6$. In these materials the planar copper (Cu(2)) and oxygen (O(2) and O(3)) atoms are separated by 1.945Å and 1.964Å because of their slightly rectangular coordination. Bates (1989) deduced from a lattice dynamical model of NiO and obtained the force constants of $152Nm^{-1}$ and $149Nm^{-1}$, respectively for these two bonds. These values are more than twice the values found for k_1 and k_2 in this work despite the similar bond lengths. We believe that most of this discrepancy is made up by the angular contributions (for example k_3 and k_7) that are present in the VFF model.

3) Two phonon scattering

The Raman spectrum of CuO for the frequency region extending from about $100cm^{-1}$ to $1400cm^{-1}$ is shown in Figures 4.6. A relatively broad peak at $1100cm^{-1}$ is observed. At room temperature it has an onset at about $1050cm^{-1}$, it peaks at about $1120cm^{-1}$ and decreases rapidly at about $1240cm^{-1}$. At 15K these frequencies are increased by about $6cm^{-1}$, slightly larger than the one phonon increases (~4-$5cm^{-1}$, Table 4.1). The temperature character of this feature is similar to that of the phonon

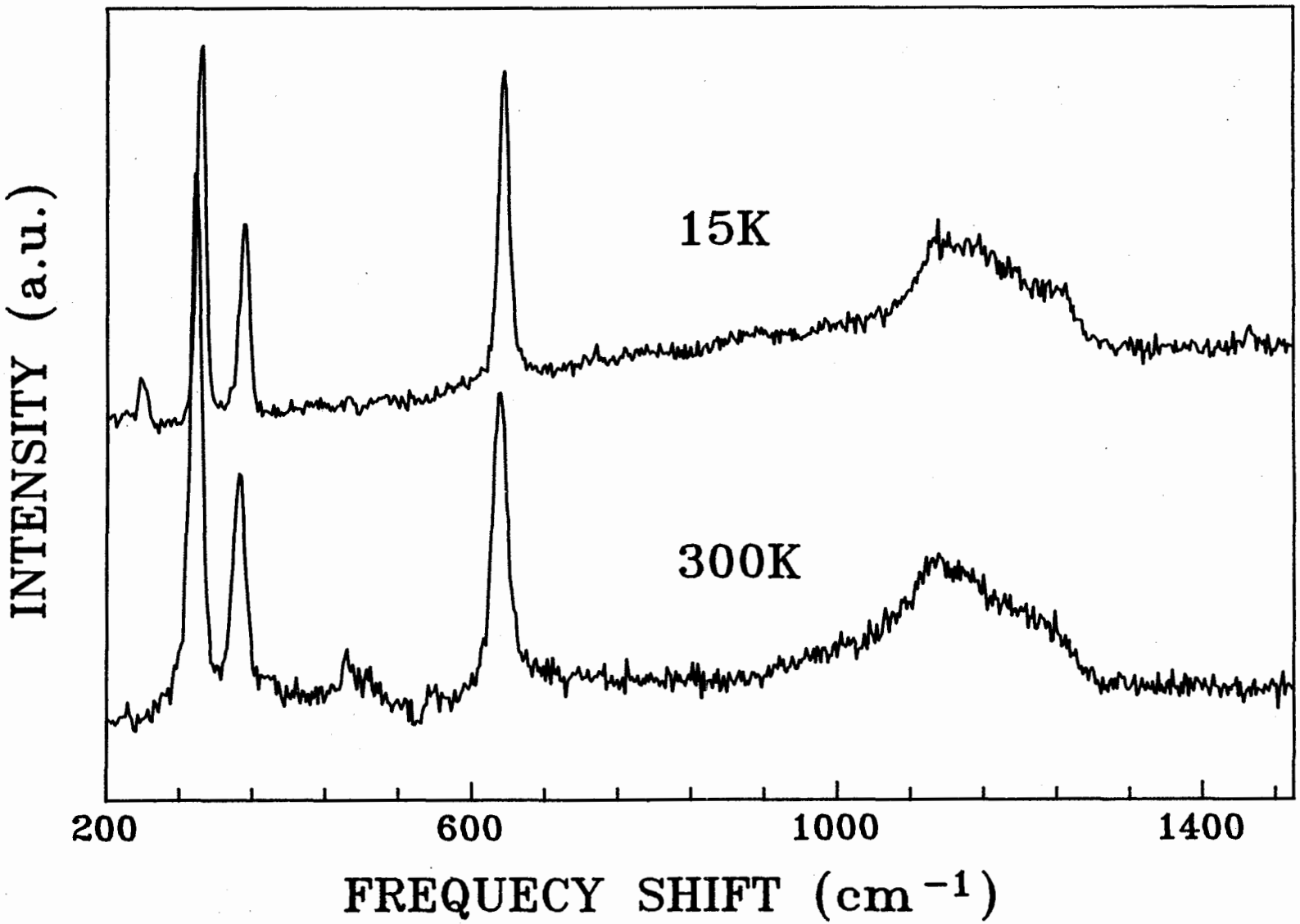

Fig.4.6 Unpolarized Raman spectra at 15K and room temperature showing the multi-phonon feature at about 1100cm^{-1}.

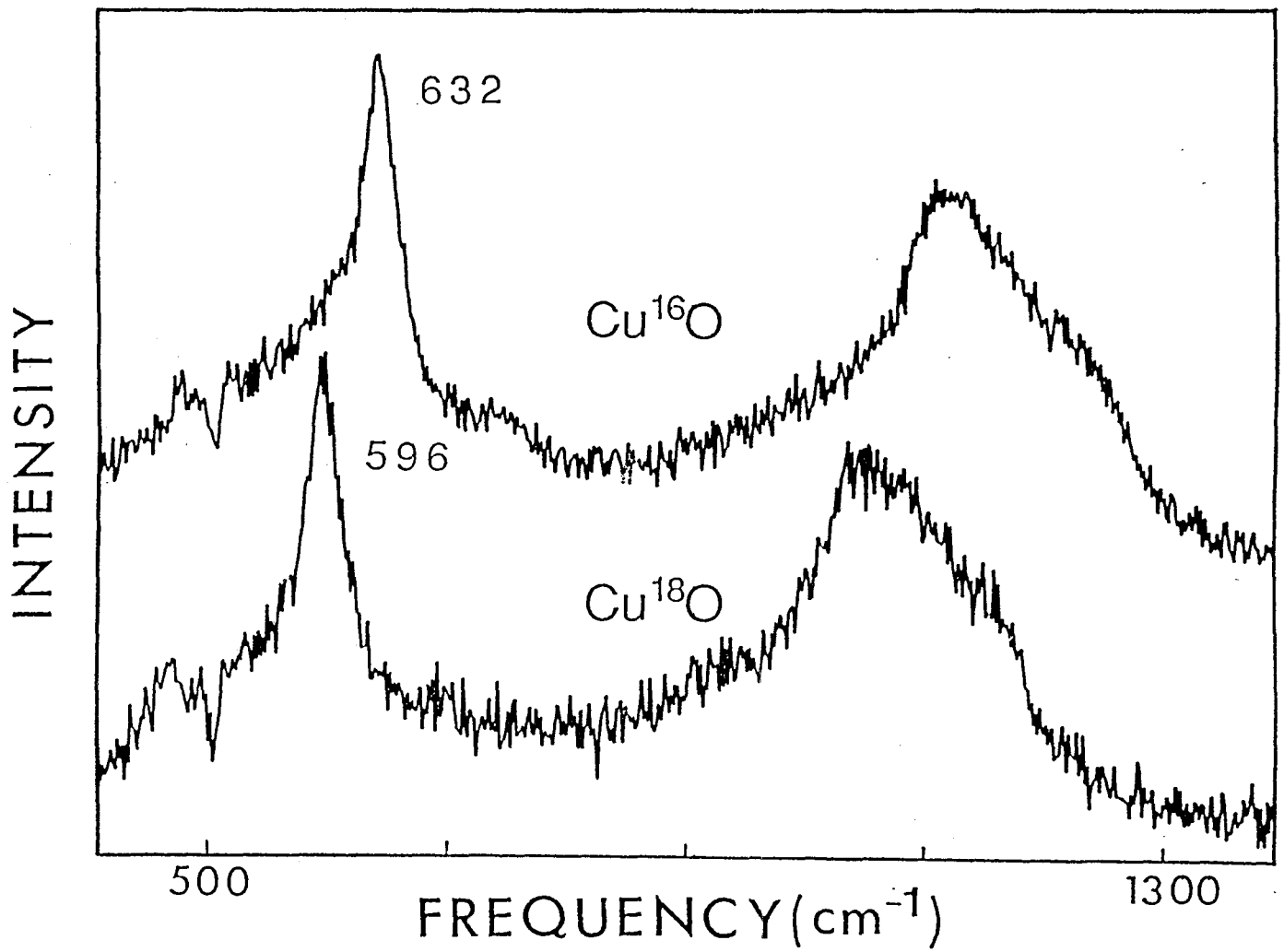

Fig.4.7 Room temperature Raman spectra of CuO (upper trace) and $Cu^{18}O$ (Lower trace) in the spectral region from about 450cm^{-1} to 1300cm^{-1} showing the shift of the two-phonon feature at 1150cm^{-1}. The dip in the spectra at about 500cm^{-1} is an experimental artifact. The two spectra are vertically displaced for clarity.

scattering, that is, the frequency is increased when the crystal is cooled (Chapter 4.1). Furthermore, a similar feature is observed in the spectrum obtained from $Cu^{18}O$ (Fig.4.7), and a comparison with the CuO spectrum shows that the peak has shifted to a lower frequency. The measured frequency shift of about $70cm^{-1}$ is about twice that of the isotopically induced one phonon shift of the $630cm^{-1}$ mode (Fig.4.5). This peak is thus assumed to be due to two phonon overtones of the vibrational modes near $600cm^{-1}$.

Considering the density of phonon states in CuO given by Reichardt et al. (1990), there exists a non-zero density of states region beginning at about $520cm^{-1}$ and ending at $640cm^{-1}$, with two peaks centered at about $565cm^{-1}$ and $620cm^{-1}$. Thus two phonon scattering coming from this region should begin at about $1040cm^{-1}$ and end at $1280cm^{-1}$ with maxima at $1130cm^{-1}$ and $1240cm^{-1}$. This general description is in excellent agreement with the observed shape of peak. It is thus concluded that the $1100cm^{-1}$ peak is a two-phonon scattering peak representing two-phonon overtones of phonons in the region of $520cm^{-1}$ to $640cm^{-1}$.

4) $2200cm^{-1}$ peak

Fig.4.8 shows the Raman spectra of CuO at 300K and 15K in the frequency region between $100cm^{-1}$ and 6000^{-1}. A very interesting feature

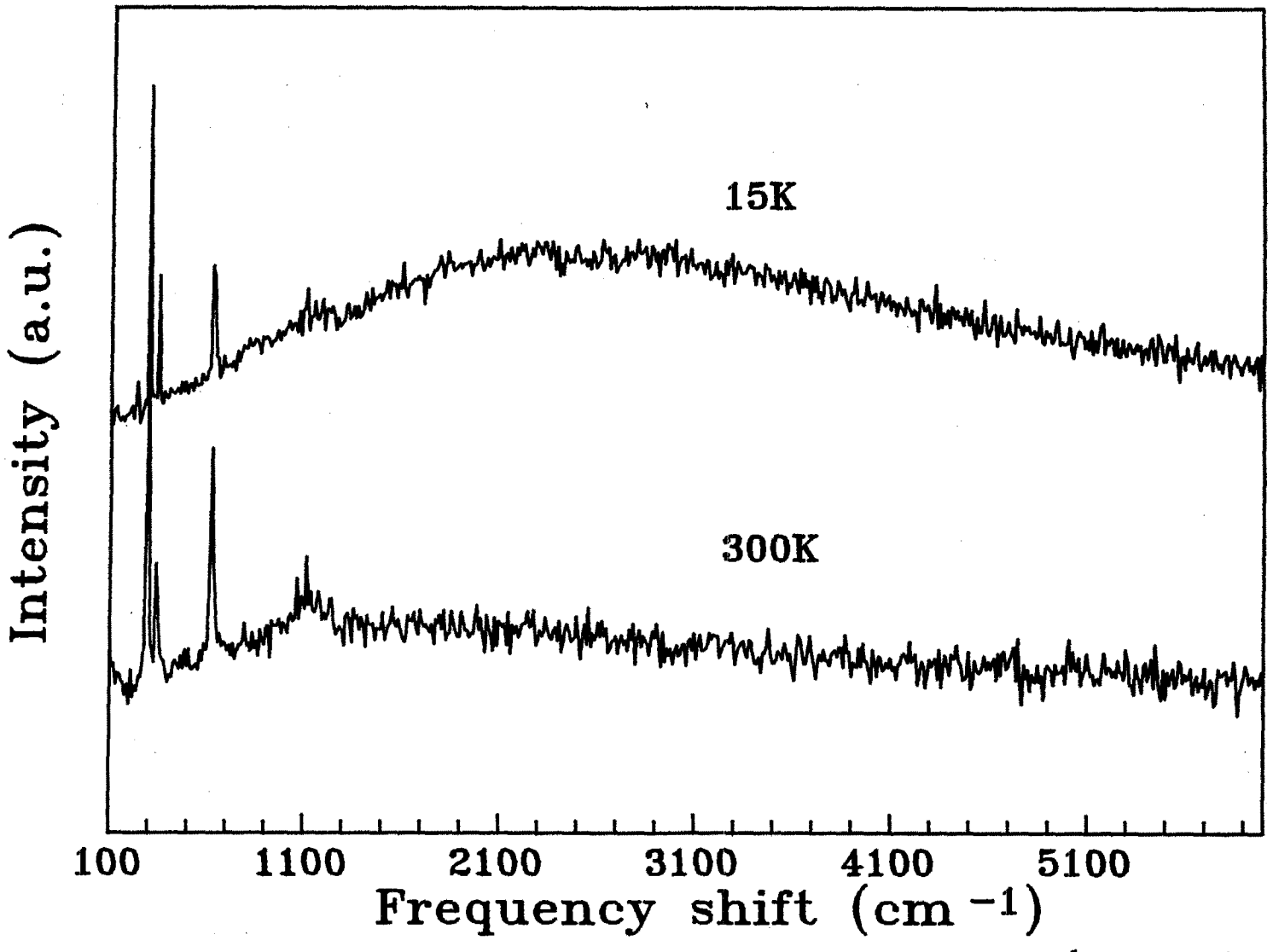

Fig.4.8 Raman spectra of CuO at 15K and 300K in the frequency region 100-6000cm^{-1}. Obtained from the double grating spectrometer and excited by the 514.5nm line.

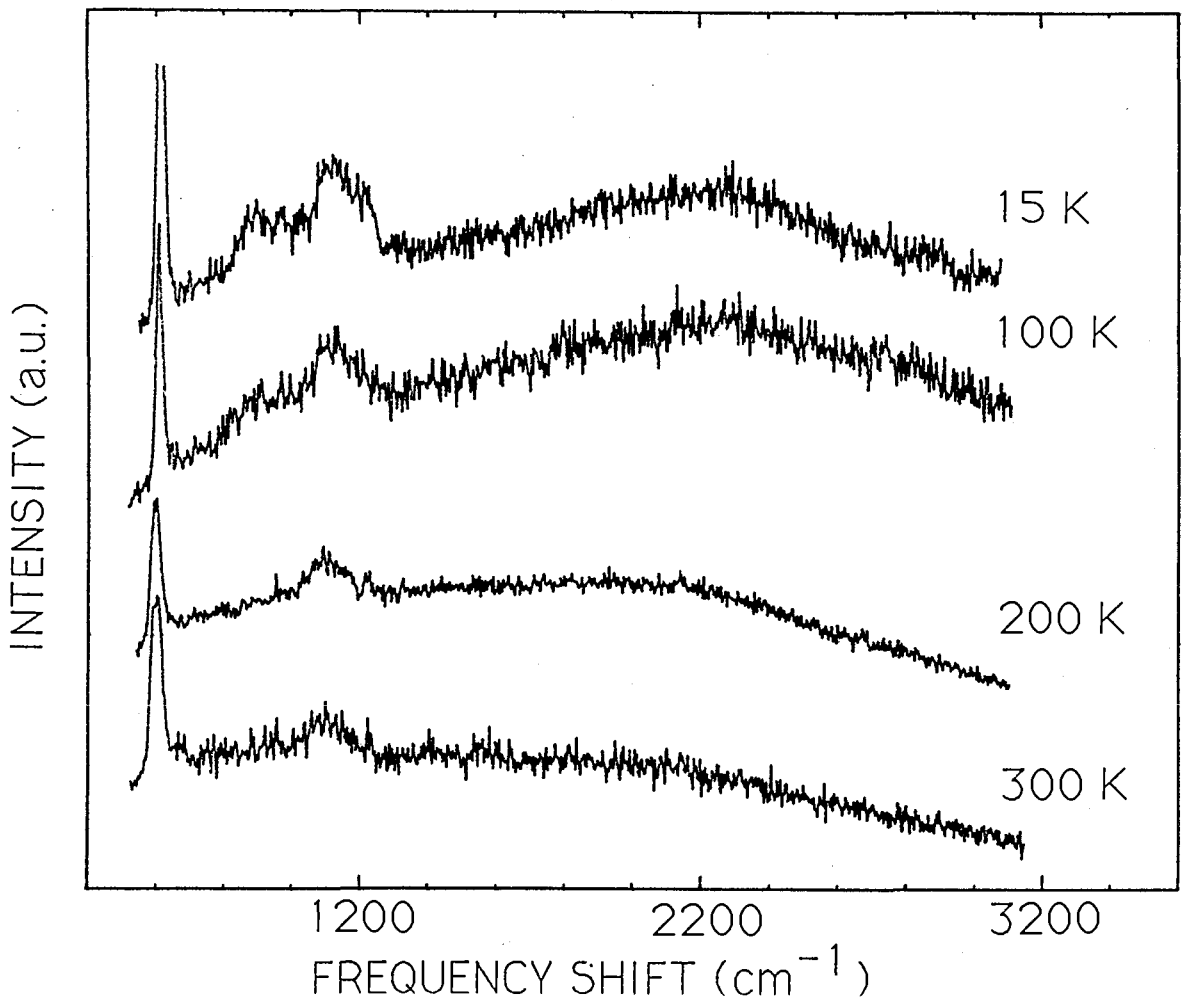

Fig.4.9 Raman spectra from an unoriented CuO crystal at various temperature.

whose occurs at about 2200cm^{-1} is observed in spectra at 15K and from Fig.4.9 one can see that this feature becomes apparent at temperatures below 200K.

A peak with similar appearance was observed in the Raman spectra of La_2CuO_4 (3000cm^{-1}) and $YBa_2Cu_3O_{6+x}$ with $x\cong 0$ (2600cm^{-1}) (Lyons et al. 1988(1) and (2)). This peak was identified by polarized measurements and by its temperature dependence as a two-magnon scattering which arises from the overtones of zone boundary magnons. They modeled their results with a 2-dimensional (2D) spin 1/2 Heisenberg model developed by Parkinson (1969). According to this model the magnon energy as a function of wave vector is given by (Lyons et al. 1988)

$$E_k^2=\{(SJZ+g\mu H_A)^2-(SJZ\gamma_k)^2\} \qquad (4.1)$$

where S is the spin, J the nearest neighbour exchange and Z is the number of nearest neighbours. The **k**-dependence is contained in γ_k which is given by

$$\gamma_k=(1/2)\{\cos(k_x a)+\cos(k_y a)\} \qquad (4.2)$$

The anisotropy field H_A is negligible in La_2CuO_4, as is in CuO. At the zone boundary $\gamma_k=0$, with Z=4 and S=1/2 the magnon frequency is given by 2J. The frequency of a two magnon peak should thus be equal to 4J. However this estimate must be altered to account for magnon-magnon interactions, Parkinson (1969) and Hayes and Loudon (1978) found that for a two-dimensional system the resulting two magnon scattering should be peaked at

$$\omega_{2m}=2.7J \qquad (4.3)$$

Using this relation Lyons et al. (1988(1)) and 1988(2)) obtained a value of $J=1100cm^{-1}$ for La_2CuO_4 and $J\cong950cm^{-1}$ for $YBa_2Cu_3O_{6+x}$ ($x\cong0$).

Obviously the $2200cm^{-1}$ peak observed in CuO is not related to phonons, as it becomes stronger when the temperature is lowered (Figs.4.8 and 4.9). If it was a two-phonon (or multi-phonon) overtone process its intensity would increase with the increasing temperature, because more phonons are involved in the process when the temperature is increased (Chapter 2.5). In addition, according to Reichardt et al. (1990), beyond $640cm^{-1}$ the density of phonon states of CuO is zero, so that at least 4 phonons are needed to produce a multi-phonon scattering at the energy range of $2200cm^{-1}$ and the isotopic frequency shift of $Cu^{18}O$ could be as large as $140cm^{-1}$ (by comparison with the two phonon process), however no such an isotopic shift is observed in $Cu^{18}O$ (Fig.4.10 is the spectrum of $Cu^{18}O$ at 50K).

Analogously it may also result from two-magnon scattering. In contrast to the scattering in the high-T_c cuprates, such as La_2CuO_4 (Lyons et al. 1988(1)), $YBa_2Cu_3O_{6+x}$ (Lyons et al. 1988(2)) and $(La_{1-x}Sr_x)_2CuO_4$ (Sugai et al. 1988), which seems to be almost independent of temperature (T<300K) consistent with scattering from low dimensional spin systems, the peak observed here depends quite strongly on the temperature. At room temperature this peak is almost invisible

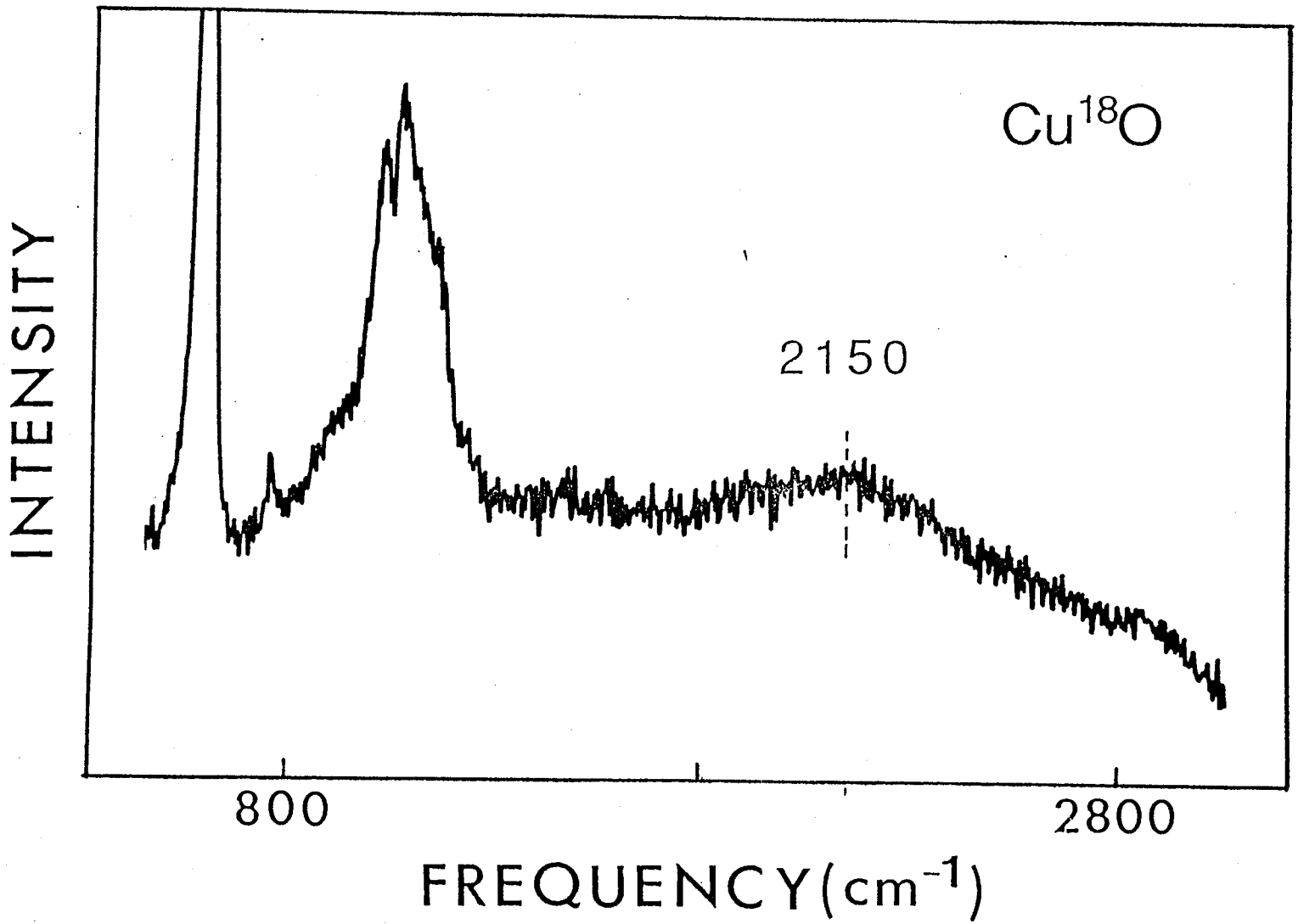

Fig.4.10. Raman spectrum of $Cu^{18}O$ obtained with the 488.0nm line and the sample at a temperature of about 50K in the region of excitation.

and it becomes much stronger as the ambient temperature is lowered to about 100K, and then remains relatively constant as the temperature is lowered further, thus appearing only when the temperature is lower than Néel temperature T_N=212K. This behavior is more typical of two magnon scattering in a 3-dimensional system than that of a 2-dimensional system (Cottam and Lockwood 1986).

In CuO this scattering is peaked at about 2200cm^{-1}, which is a smaller energy than the scattering peak observed in other cuprates. The magnetic structure of CuO is not known for $T<T_N$ and thus only a very crude estimate for J can be obtained. If, however, CuO is assumed to be a two-dimensional system and that Z=4, S=1/2, from Eq.(4.3) magnetic interactions lead to a similar estimate for J of J≅800cm^{-1} or about 100meV. This is in reasonable agreement with the value of 80meV obtained by Ain et al. (1989) from neutron scattering experiments. Ain et al. (1989) also estimated the magnon density of states from their neutron scattering results. They found that the density of states could be characterized as a plateau ranging from 700cm^{-1} to 1200cm^{-1}, a broad peak around 1350cm^{-1} and a high-frequency cut-off near 1500cm^{-1}. If the magnon-magnon interactions are considered, ascribing the 2200cm^{-1} peak as a two-magnon scattering is again consistent with the results of Ain et al..

The above consideration is only a qualitativel estimate. Singh et

al. (1989) have suggested that the magnetic properties of the crystals may be poorly represented by a simple spin wave picture, and a quantum fluctuation mechanism was proposed. Recently, Lyons et al. (1989) found that intraband electronic excitations might also contribute to the scattering in La_2CuO_4, so it is also possible that the electronic mechanism plays an important role in the scattering in CuO. Obviously, to further identify the origin of this peak, more experimental results and quantitative calculations are needed.

One other feature of the spectra shown in Fig.4.5 remains puzzling. The peak at 465cm^{-1} is present in both the CuO and $Cu^{18}O$ spectra obtained from powders. This peak thus can not arise from any vibration involving oxygen and furthermore can not arise from any oxide impurity. It is tempting to assign it to some form of magnetic excitation but there is no observed scattering at this frequency in spectra obtained from single crystals (Irwin et al. 1990). This feature is thus tentatively assigned to some unknown impurity that is present in both the CuO and $Cu^{18}O$ powders.

Another interesting feature which we will not discuss in detail is the 240cm^{-1} mode observed at low temperatures (Fig.4.1). It was attributed to a magnetic exciton by Chrzanowski and Irwin (1989), and later experimental results were consistent with this interpretation (Irwin et al. 1990).

5. CONCLUSIONS

Raman scattering experiments have been carried out on CuO crystals and $Cu^{18}O$ powder pellets. The symmetries of three phonon modes have been determined with the help of polarized spectra. The results were used to determine force constants in a simple valence-force-field (VFF) lattice dynamical model. 11 force constants are calculated, 7 of them represent the nearest neighbor interactions and 4 stretch force constants are second and third neighbor interactions. The Raman frequencies of $Cu^{18}O$ predicted by this model are in excellent agreement with the experimental results, and thus lend confidence to the model. Further work should include the addition of long range Coulomb forces to the VFF model used in this work.

The force constants obtained are qualitatively consistent with other dynamical models (Reichardt et al. 1990, Guha et al. 1990). The stretch force constants of the shortest Cu-O bonds obtained are found to be much less than equivalent bonds in $YBa_2Cu_3O_7$ and $YBa_2Cu_3O_6$ (which were estimated from a dynamical model of NiO (Bates 1989)), but most of the discrepancy may be made up by the angular contributions.

The origin of a relatively broad peak at $1100cm^{-1}$ is revealed as two-phonon scattering by comparing with Raman spectrum of $Cu^{18}O$ and the density of phonon states obtained from neutron scattering measurements.

This result implies that the features observed in the undoped cuprates $YBa_2Cu_3O_6$ (Lyons et al. 1988(1)), La_2CuO_4 (Lyons et al. 1988(2)) and $(La_{1-x}Sr_x)_2CuO_4$ (Sugai et al. 1988), which have a very similar energy ($\sim 1400 cm^{-1}$) and shape may also be vibrational in origin, and not magnetic as was suggested by some researchers (Ohana et al. 1989 and Zeiger et al. 1989).

A very broad feature centered at about $2200 cm^{-1}$ is observed in the Raman spectrum of CuO. The frequency and lineshape of this feature are also very similar to features observed in the Raman spectra of the undoped high-T_c cuprates. Ascribing it to two-magnon scattering is consistent with neutron experimental results. However, further work, including a determination of the magnetic structure in CuO, will be required before a definitive description of this scattering can be formulated.

Since there exists the possibility that magnetic properties play an important role in the high-T_c mechanism, antiferromagnetic effects in many high-T_c cuprates are attracting a great deal of attention. Investigations of the magnetic excitations in CuO involves the study of spin-1/2 antiferromagnetic system which has been found to have properties in accord with a 1-dimensional system (Yang et al. 1989 and Loram et al. 1989), a 1-dimensional X-Y model (Gmelin et al. 1990), and a 3-dimensional system (Ain et al. 1990 and this work). The exact nature

of the antiferromagnitically ordered state of CuO may in fact not be very well represented by a simple spin wave model as suggested by our previous results (Irwin et al. 1990) and by recent theoretical considerations of the high-T_c cuprates. Hagemann et al. (private communication) have carried out Raman scattering experiments in a magnetic field which tend to confirm the interpretation of the 240cm^{-1} peak as a magnetic exciton. It would also be interesting to carry out experiments on $Cu_{1-x}Zn_xO$, for example, to investigate the effects of such doping on the two-magnon scattering observed in this work.

Further investigations of the magnetic properties of CuO are however not only of interest in elucidating the properties of this relatively simple compound, but also because of their relevance to high temperature superconductors. The undoped cuprates have properties that are very similar to those of CuO and it is possible that magnetic interaction could play a role in high temperature superconductivity.

Appendix 1. Matrix forms of force constants

In this work, the x and y axes are chosen to lie along a and b axes of the unit cell of CuO, respectively, and the primitive cell is chosen as shown in Fig.2.1. We denote two copper atoms as no.1 and no.2 atoms in the cell, and two oxygen atoms as no.3 and no.4. Other equivalent atoms in adjacent cells are labeled by the same number with a subscript.

Eq.2.7 shows that to construct the dynamical matrix M and thus calculate phonon frequencies, it is necessary to consider the interactions between atoms in the primitive cell and any other atom in the crystal. In the following treatment of CuO, the nearest neighbor interactions, that is, the shortest Cu-O bonds (1.95Å and 1.96Å), and the shortest bonds between oxygen atoms, O-O (2.62Å) and other Cu-Cu (3.08Å, 3.17Å and 3.75Å) bonds, are taken into consideration.

First let us consider the nearest neighbor interactions, and write the force constant matrices between O3 and Cu1, and O3 and Cu1" as

$$-\phi(3,1)=\begin{pmatrix} \alpha_{11} & \alpha_{12} & \alpha_{13} \\ \alpha_{21} & \alpha_{22} & \alpha_{23} \\ \alpha_{31} & \alpha_{32} & \alpha_{33} \end{pmatrix} \qquad \text{(A1.1)}$$

$$-\phi(3,1")=\begin{pmatrix} \beta_{11} & \beta_{12} & \beta_{13} \\ \beta_{21} & \beta_{22} & \beta_{23} \\ \beta_{31} & \beta_{32} & \beta_{33} \end{pmatrix} \qquad \text{(A1.2)}$$

Then the translational invariance results in that the force

constant between O3′ and Cu1" is

$$-\phi(3',1")=-\phi(3,1)=\begin{pmatrix} \alpha_{11} & \alpha_{12} & \alpha_{13} \\ \alpha_{21} & \alpha_{22} & \alpha_{23} \\ \alpha_{31} & \alpha_{32} & \alpha_{33} \end{pmatrix} \qquad \text{(A1.3)}$$

Since the force constant matrices are invariant under the symmetry operations (Maradudin et al. 1971) of the crystal.

Notice that the operation $C_2[010]$ located at O3 brings Cu1 to Cu2 and Cu1" to Cu2′, but leaves O3 unchanged. By applying the transformation rules (Maradudin et al. 1971), we have

$$-\phi(3,2)=S_2(-\phi(3,1))S_2^{-1}$$

$$=\begin{pmatrix} \alpha_{11} & -\alpha_{12} & \alpha_{13} \\ -\alpha_{21} & \alpha_{22} & -\alpha_{23} \\ \alpha_{31} & -\alpha_{32} & \alpha_{33} \end{pmatrix} \qquad \text{(A1.4)}$$

and $$-\phi(3,2')=S_2(-\phi(3,1"))S_2^{-1}$$

$$=\begin{pmatrix} \beta_{11} & -\beta_{12} & \beta_{13} \\ -\beta_{21} & \beta_{22} & -\beta_{23} \\ \beta_{31} & -\beta_{32} & \beta_{33} \end{pmatrix} \qquad \text{(A1.5)}$$

where $S_2=\tilde{S}_2=S_2^{-1}=\begin{pmatrix} -1 & & \\ & 1 & \\ & & -1 \end{pmatrix}$ is the unitary matrix of operation $C_2[010]$.

Similarly, the consideration of operation C_i (with $S_i = \tilde{S}_i = S_i^{-1} = \begin{pmatrix} -1 & & \\ & -1 & \\ & & -1 \end{pmatrix}$) at Cu2 gives rise $-\phi(4,2')=-\phi(3,2)$ and $-\phi(4,2)=-\phi(3,2')$, C_2 at O4 gives rise $-\phi(4,1"^a)=-\phi(3,1)$ and $-\phi(4,1^a)=-\phi(3,1")$.

Considering the interaction between O3 and O4 (2.62Å). As $\phi(1\kappa,1'\kappa')=\tilde{\phi}(1'\kappa',1\kappa)$, the operation C_i at Cu2 and translational invariance result in $\phi(3,4)$ being symmetric, i.e., it can be written as $\begin{pmatrix} \delta_{11} & \delta_{12} & \delta_{13} \\ \delta_{12} & \delta_{22} & \delta_{23} \\ \delta_{13} & \delta_{23} & \delta_{33} \end{pmatrix}$ (i.e., the Eq.2.10e). And from this form of $\phi(3,4)$, $\phi(3,4^a)=\begin{pmatrix} \delta_{11} & -\delta_{12} & \delta_{13} \\ -\delta_{12} & \delta_{22} & -\delta_{23} \\ \delta_{13} & -\delta_{23} & \delta_{33} \end{pmatrix}$ (Eq.2.10f) is obtained by applying the C_i operation at O3.

With the force constant between two closest copper atoms $\phi(1,2')$ (3.08A) is written as $\begin{pmatrix} \eta_{11} & \eta_{12} & \eta_{13} \\ \eta_{21} & \eta_{22} & \eta_{23} \\ \eta_{31} & \eta_{32} & \eta_{33} \end{pmatrix}$ (Eq.2.10g), operation C_2 located at O3 results in $\phi(1,2^c)=\begin{pmatrix} \eta_{11} & -\eta_{21} & \eta_{31} \\ -\eta_{12} & \eta_{22} & -\eta_{32} \\ \eta_{13} & -\eta_{23} & \eta_{33} \end{pmatrix}$ (Eq.2.10h). There are two other Cu-Cu bonds with the same distance as Cu1-Cu2' which stretch outside Fig.2.1, and it can be proven that one equals to $\phi(1,2')$ and another equals to $\phi(1,2^c)$.

The dynamical matrix can be written as

$$M=\begin{pmatrix} M(1,1) & M(1,2) & M(1,3) & M(1,4) \\ M(2,1) & M(2,2) & M(2,3) & M(2,4) \\ M(3,1) & M(3,2) & M(3,3) & M(3,4) \\ M(4,1) & M(4,2) & M(4,3) & M(4,4) \end{pmatrix} \qquad \text{(A1.6)}$$

where each $M(\kappa,\kappa')$ is a 3×3 matrix. M(3,1), for example, represents interactions between all copper atoms in the crystal denoted by 1 and the atom no.3 (O3) in the considered primitive cell.

If only the first and second neighbor interactions are included in

the calculation, by defining $(\gamma)_{3x3} \equiv (\alpha)_{3x3} + (\beta)_{3x3}$, we have

$$M_{\alpha\beta}(3,1) \equiv M(3\alpha,1\beta) = \phi_{\alpha\beta}(3,1) + \phi_{\alpha\beta}(3,1') = -\gamma_{\alpha\beta} \tag{A1.7}$$

with $(\alpha,\beta=1,2,3)$

$$M(3,2) \equiv \phi(3,2) + \phi(3,2') = -\begin{pmatrix} \gamma_{11} & -\gamma_{12} & \gamma_{13} \\ -\gamma_{21} & \gamma_{22} & -\gamma_{23} \\ \gamma_{31} & -\gamma_{32} & \gamma_{33} \end{pmatrix} \tag{A1.8}$$

$$M_{\alpha\beta}(4,1) = \phi_{\alpha\beta}(4,1'') + \phi_{\alpha\beta}(4,1''^{a}) = -\gamma_{\alpha\beta} \tag{A1.9}$$

$$M_{\alpha\beta}(4,2) = \phi_{\alpha\beta}(4,2) + \phi_{\alpha\beta}(4,2') = M_{\alpha\beta}(3,2) \tag{A1.10}$$

$$M(3,4) = \phi(3,4) + \phi(3,4^{a}) = -2\begin{pmatrix} \delta_{11} & & \delta_{13} \\ & \delta_{22} & \\ \delta_{13} & & \delta_{33} \end{pmatrix} \tag{A1.11}$$

and

$$M(1,2) = 2(\phi(1,2') + \phi(1,2^{c}) = -2\begin{pmatrix} 2\eta_{11} & \eta_{12}-\eta_{21} & \eta_{13}+\eta_{31} \\ \eta_{21}-\eta_{12} & 2\eta_{22} & \eta_{23}-\eta_{32} \\ \eta_{31}+\eta_{13} & \eta_{32}-\eta_{23} & 2\eta_{33} \end{pmatrix} \tag{A1.12}$$

Since matrix M is hermitian, at q=0 it is symmetric, that is, $M(\kappa,\kappa') = \tilde{M}(\kappa',\kappa)$. Using the above 6 equations (A1.7) to (A1.12), the form of M except diagonal blocks (M(i,i), i=1,2,3 and 4) is thus obtained.

To calculate the diagonal blocks, let us consider a uniform translation of the whole crystal, that cannot produce a force on any atom, that is,

$$\sum_{1'\kappa'} \phi_{\alpha\beta}(1\kappa,1'\kappa') = 0 \tag{A1.13}$$

or

$$\sum_{\kappa'} M(\kappa\alpha,\kappa'\beta) = 0 \tag{A1.14}$$

and the elements in diagonal blocks can be calculated by

$$M(\kappa\alpha,\kappa'\beta) = -\sum_{\kappa'\neq\kappa} M(\kappa\alpha,\kappa'\beta) \tag{A1.15}$$

Thus the dynamical matrix can be written as Eq.(2.14).

Because the matrix M is symmetric, from the form of M, we see that the following conditions must be satisfied:

$$\gamma_{21}=\gamma_{12}+\eta_{12}-\eta_{21} \qquad \text{(A1.16a)}$$

$$\gamma_{32}=\gamma_{23}+\eta_{23}-\eta_{32} \qquad \text{(A1.16b)}$$

$$\gamma_{31}=\gamma_{13} \qquad \text{(A1.16c)}$$

As is mentioned above, only nearest and second nearest neighbor interactions are included in Table 2.1. However, with further study of the symmetries of the crystal, it could be found that the form of Eq.(2.14) remained unchanged when additional the third and fourth interactions are added. But one should note that the resultant parameters α_{ij},β_{ij},δ_{ij} and η_{ij} are changed.

Appendix 2. Valence Force Field model

In the Valence Force Field model, a bond between two atoms is treated as a spring, and the changing of a angle between two bonds is considered as a bending which results in a restoring force. The potential energy of the system is expressed as (Herzberg 1950, Wilson et al. 1955):

$$2\Phi=k_{r1}\sum_i(\Delta r_{1i})^2+k_{r2}\sum_i(\Delta r_{2i})^2+\cdots$$
$$+k_{\psi 1}\sum_j r_{1j}^{(1)}r_{2j}^{(1)}(\Delta\psi_{1j})^2+k_{\psi 2}\sum_j r_{1j}^{(2)}r_{2j}^{(2)}(\Delta\psi_{2j})^2+\cdots \tag{A2.1}$$

where Δr_{si} are the stretch of bonds being considered, $\Delta\psi_{tj}$ the change of angle between bonds $r_{1j}^{(t)}$ and $r_{2j}^{(t)}$, k_{rs} are known as the stretch force constants and $k_{\psi t}$ (or $k_{\psi t}r_{1j}^{(t)}r_{2j}^{(t)}$ used by some writers) as bending force constants, where s, t=1, 2, 3, ····.

With this expression of potential energy, the "general" force constants can be calculated from Eq.(2.3)

$$\phi_{\alpha\beta}(l\kappa,l'\kappa')=\left(\frac{\partial^2\Phi}{\partial u_\alpha(l\kappa)\partial u_\beta(l'\kappa')}\right)_0 \tag{A2.2}$$

where $u_\alpha(l\kappa)$ are displacements of atoms (α,β=1,2,3).

Considering a string between two atoms i and j (Fig.2.4), the stretch potential energy is

$$\Phi=\frac{1}{2}k_s|R_i-R_j|^2=\frac{1}{2}k_s|u_i-u_j|^2 \tag{A2.3}$$

where R_i and R_j are positions of atoms. The force constant matrix ϕ^s is easy to derive:

$$\phi^s = -k_s \begin{pmatrix} \cos^2\alpha_1 & \cos\alpha_1\cos\beta_1 & \cos\alpha_1\cos\gamma_1 \\ \cos\alpha_1\cos\beta_1 & \cos^2\beta_1 & \cos\beta_1\cos\gamma_1 \\ \cos\alpha_1\cos\gamma_1 & \cos\beta_1\cos\gamma_1 & \cos^2\gamma_1 \end{pmatrix} \tag{A2.4}$$

where α_1, β_1 and γ_1 are angles between the bond and cartesian axes x, y and z, respectively.

Now we try to derive $\phi_{\alpha\beta}$ from bending force constant k_ψ:

$$\Phi = \frac{1}{2} k_\psi x_0 x_0' (\Delta\psi)^2 \tag{A2.5}$$

where $x_0 = |R_{ji}|$ and $x_0' = |R_{ki}|$, R_{ji} and R_{ki} are equilibrium position vectors shown in Fig.2.5a. Suppose that the positions of atoms are shifted to that in Fig.2.5b after a vibration, we have

$$\cos\psi = \frac{(R_{ji}+u_{ji})\cdot(R_{ki}+u_{ki})}{|R_{ji}+u_{ji}|\cdot|R_{ki}+u_{ki}|} \tag{A2.6}$$

to the first order

$$\cos\psi = (x_0 x_0'\cos\psi_0 + R_{ki}\cdot u_{ji} + R_{ji}\cdot u_{ki})\frac{1}{x_0 x_0'}\left(1-\frac{R_{ji}\cdot u_{ji}}{x_0^2}\right)\left(1-\frac{R_{ki}\cdot u_{ki}}{x_0'^2}\right)$$

$$= \frac{1}{x_0 x_0'}\left[x_0 x_0'\cos\psi_0 + \left(R_{ki} - \frac{x_0'}{x_0}R_{ji}\cos\psi_0\right)\cdot u_{ji} + \left(R_{ji} - \frac{x_0}{x_0'}R_{ki}\cos\psi_0\right)\cdot u_{ki}\right] \tag{A2.7}$$

but $\cos\psi = \cos(\psi_0+\Delta\psi) = \cos\psi_0\cos(\Delta\psi) - \sin\psi_0\sin(\Delta\psi)$

$$\cong\cos\psi_0(1-(\Delta\psi)^2/2)-\sin\psi_0(\Delta\psi)\cong\cos\psi_0-\sin\psi_0(\Delta\psi) \qquad \text{(A2.8)}$$

i.e. $$\Delta\psi=\frac{\cos\psi_0-\cos\psi}{\sin\psi_0} \qquad \text{(A2.9)}$$

$$\therefore \quad \Phi_b=\frac{1}{2}k_\psi x_0 x_0'\left(\frac{\cos\psi_0-\cos\psi}{\sin\psi_0}\right)^2 \qquad \text{(A2.10)}$$

In CuO, $x_0(1.95\text{Å})\cong x_0'(1.96\text{Å})$, the potential energy may thus be approximately written as

$$\Phi_b\cong\frac{k_\psi}{2x_0^2\sin^2\psi_0}\left[(R_{ki}-R_{ji}\cos\psi_0)\cdot(u_j-u_i)+(R_{ji}-R_{ki}\cos\psi_0)\cdot(u_k-u_i)\right]^2 \qquad \text{(A2.11)}$$

The force constant matrix element expressed in bending force constant k_ψ is then derived from Eq.(A2.2):

$$\phi^b_{\alpha\beta}(i,j)=-\frac{k_\psi}{x_0^2(1+\cos\psi_0)}(R^\alpha_{ki}+R^\alpha_{ji})(R^\beta_{ki}-R^\beta_{ji}\cos\psi_0) \qquad \text{(A2.12)}$$

and $$\phi^b_{\alpha\beta}(k,j)=\frac{k_\psi}{x_0^2\sin\psi_0}(R^\alpha_{ji}-R^\alpha_{ki}\cos\psi_0)(R^\beta_{ki}-R^\beta_{ji}\cos\psi_0) \qquad \text{(A2.13)}$$

If all stretch and bending force constants k_i are defined, as the positions of atoms and angle between bonds are known, the expression of all force constant matrix elements, which are needed for the dynamical matrix M, in terms of k_i (i=1, 2, $\cdots$,11) can be obtained by applying the above two equations. A simple BASIC program was made for this

purpose, and with the force constants defined as shown in Figs.2.6 and 2.7 and Table 2.2 the numerical results are obtained as:

$$-\begin{pmatrix} \gamma_{11} & \gamma_{12} & \gamma_{13} \\ \gamma_{21} & \gamma_{22} & \gamma_{23} \\ \gamma_{31} & \gamma_{32} & \gamma_{33} \end{pmatrix} = k_1 \begin{pmatrix} .4911 & -.2074 & -.4549 \\ -.2074 & .0876 & .1921 \\ -.4549 & .1921 & .4214 \end{pmatrix} + k_2 \begin{pmatrix} .2484 & -.2886 & .3216 \\ -.2886 & .3353 & -.3736 \\ .3216 & -.3736 & .4162 \end{pmatrix}$$

$$+k_3 \begin{pmatrix} .0481 & .0692 & -.3134 \\ .0692 & .0996 & -.4510 \\ -.3134 & -.4510 & 2.0421 \end{pmatrix} - k_4 \begin{pmatrix} 2.3513 & 1.0477 & \\ -.0567 & .1338 & .3693 \\ & & \end{pmatrix}$$

$$-k_5 \begin{pmatrix} & & \\ .4113 & 1.8375 & -.3810 \\ & & \end{pmatrix} - k_6 \begin{pmatrix} & & \\ .5797 & 1.3163 & .7503 \\ & & \end{pmatrix}$$

$$-k_7 \begin{pmatrix} 1.1738 & -.8578 & \\ -.8578 & .6268 & \\ & & \end{pmatrix} \qquad \text{(A2.14a)}$$

$$-2\begin{pmatrix} \delta_{11} & & \delta_{13} \\ & \delta_{22} & \\ \delta_{13} & & \delta_{33} \end{pmatrix} = k_7 \begin{pmatrix} 1.1257 & & .3134 \\ & .5272 & \\ .3134 & & -2.0420 \end{pmatrix} - k_{10} \begin{pmatrix} .0439 & & -.2862 \\ & .0910 & \\ .2862 & & 1.8651 \end{pmatrix}$$

(A2.14b)

$$-\begin{pmatrix} 2\eta_{11} & \eta_{12}-\eta_{21} & \eta_{13}+\eta_{31} \\ \eta_{21}-\eta_{12} & 2\eta_{22} & \eta_{23}-\eta_{32} \\ \eta_{31}+\eta_{13} & \eta_{32}-\eta_{23} & 2\eta_{33} \end{pmatrix} = k_4 \begin{pmatrix} 1.1636 & -.5522 & .0782 \\ .5522 & -.1665 & -.1846 \\ .0782 & .1846 & -.5097 \end{pmatrix}$$

$$+k_5 \begin{pmatrix} -.0460 & .2057 & .0427 \\ -.2057 & .9187 & .1905 \\ .0427 & -.1905 & -.0395 \end{pmatrix} + k_6 \begin{pmatrix} -.1276 & .2898 & -.1652 \\ -.2898 & .6582 & -.3752 \\ -.1652 & .3752 & -.2138 \end{pmatrix}$$

$$-k_8 \begin{pmatrix} .0318 & & -.2072 \\ & .6182 & \\ -.2072 & & 1.3500 \end{pmatrix} - k_9 \begin{pmatrix} .3738 & & .4838 \\ & & \\ .4838 & & .6262 \end{pmatrix}$$

$$-k_{11} \begin{pmatrix} .5382 & & -.4985 \\ & & \\ -.4985 & & .4618 \end{pmatrix} \qquad \text{(A2.14c)}$$

With all these matrices and the expression of M in Appendix 1, the dynamical matrix M expressed in terms of stretch and bending force constant k_i (i=1, 2, $\cdots$, 11) is obtained.

It can be also proved that the requirement (A1.17) is satisfied, i.e., the expression of M is self consistent. The frequency of phonons can thus be calculated provided all k_i are known.

REFERENCES

M. Ain, W. Reichardt, B. Hennion, G. Pepy and B. M. Wanklyn, Phyisca **C162-164** (1989) 1279

S. Åsbrink and L. -J. Norrby, Acta. Cryst. **B26** (1970) 8

F. E. Bates, Phys. Rev. **B39** (1989) 322

J. G. Bednorz and K. A. Müller, Z. Phys. **B64** (1986) 189

B. J. Berenblut, P. Dawson and G. R. Wilkinson, Spectrochim. Acta **27A** (1971) 1849

J. L. Birman, in Dynamical Properties of Solids, Vol.1, ed. G. K. Horton and A. A. Maradudin (North-Holland, Amsterdam, 1974)

M. Born and K. Huang, Dynamical Theory of Crystal Lattices (Clarendon, Oxford, 1954)

P. Brüesch, Phonons: Theory and Experiments I (Springer-Verlag, Berlin, 1982)

P. Brüesch, Phonons: Theory and Experiments II (Springer-Verlag, Berlin, 1986)

M. Cardona, in Light Scattering in Solids II ed. M. Cardona and G. Güntherodt (Springer-Verlag, Berlin, 1982)

J. Chrzanowski and J. C. Irwin, Solid State Comm., **70** (1989) 11

W. Cochran, in Phonons, ed. R. W. H. Stevenson (Plenum, New York, 1966)

M. G. Cottam and D. J. Lockwood, Light Scattering in Magnetic Solids (Wiley, New York, 1986)

R. A. Cowley, in The Raman Effect, Vol.1, ed. A. Anderson (Marcel

Dekker, New York, 1971)

L. Degiorgi, E. Kaldis and P. Wachter, Physica **C153-155** (1988) 657

W. Desisto, B. T. Collins, R. Kershaw, K. Dwight and A. Wold, Mater. Res. Bull. **24** (1989) 1055

W. G. Fateley, F. R. Dollish, N. T. Devitt, and F. F. Bentley, Infrared and Raman Selection Rules for Molecular and Lattice Vibrations: The Correlation Method (Wiley, New York, 1972)

D. Ginsberg, in Physical Properties of High-T_c Superconductors, ed. D. Ginsberg (World Scientific, Singapore, 1989)

E. Gmelin, U. Kobler, W. Brill, T. Chattopadhyay and S. Sastry (1990), to be publised.sed.

H. F. Goldstein, Dai-sik Kim, Peter Y. Yu, L. C. Buorne, J-P. Chaminade and Leod Nganga, Phys. Rev. **B41** (1990) 7192

S. Guha, D. Peebles and J. J. Wieting, Preprint submitted to Phys. Rev.

H. Hagemann, H. Bill, W. Sadowski, E. Walker, and M. Francois, Solid State Commun. **73** (1990) 447

J. Hanuza, J. Klamut, R. Horyn and B. Jezowska-Trzebiatowska, J. Mol. Struct., **193** (1989) 57

C. E. Hathaway, in The Raman Effect, Vol.1, ed. A. Anderson (Marcel Dekker, New York, 1971)

W. Hayes and R. Loudon, Scattering of Light by Crystals (John Wiley & Sons, New York, 1978)

V. Heine, Group Theory in Quantum Mechanics (Pergamon, Oxford, 1960)

G. Herzberg, Molecular Spectra and Molecular Structure, Vol.1 (Van

Nostrand ReinHold, New York, 1950)

J. C. Irwin, J. Chrzanowski, T. Wei, D. J. Lockwood and A. Wold, Physica **C166** (1990) 456

L. D. Landau and E. M. Lifshitz, Electrodynamics of Continuous Media (Pergamon Press, New York, 1960)

J. W. Loram, K. A. Mirza, C. P. Joyce and A. J. Osborne, Eurphys. Lett. **8** (1989) 263

R. Loudon, Advan. Phys.13 (1964) 423

K. B. Lyons, P. A. Fleury, J. P. Remeika and T. J. Negran, Phys. Rev. **B37** (1988) 2353

K. B. Lyons, P. A. Fleury, L. F. Schneemeyer and J. V. Waszczak, Phys. Rev. Lett. **60** (1988) 732

K. B. Lyons, P. E. Sulewski, P. A. Fleury, H. L. Carter, A. S. Cooper, G. P. Espinosa, Z. Fisk and S. -W. Cheong, Phys. Rev. **B39** (1989) 9693

A. A. Maradudin, in Dynamical Properties of Solids, Vol.1, ed. G. K. Horton and A. A. Maradudin (North-Holland, Amsterdam, 1974)

J. T. Markert, Y. Dalichaouch and M. B. Maple, in Physical Properties of High-T_c Superconductors, ed. D. Ginsberg (World Scientific, Singapore, 1989)

J. H. Miller, Jr, in High-temperature Superconducting Materials, ed. W. E. Hatfield and J. H. Miller, Jr (Marcel Dekker, New York, 1988)

I. Ohana, M. S. Dresselhaus, Y. C. Liu, P. J. Picone, D. R. Gabbe, H. P. Jenssen and G. Dresselhaus, Phys. Rev. **B38** (1989) 2293

J. B. Parkinson, J. Phys. **C2** (1969) 2012

Z. V. Popovic, C. Thomsen, M. Cardona, R. Liu, G. Stanisic, R. Kremer and W. Konig, Solid State Comm., **66** (1988) 965

D. L. Rousseau, R. P. Bauman and S. P. S. Porto, J. Raman Spec. 10 (1981) 253

W. Reichardt, F. Gompf, M. Ain and B. M. Wanklyn, Preprint submitted to Zeit. für Phys.

P. M. A. Sherwood, Vibrational Spectrscopy of Solids (Cambridge University Press, Cambridge, 1972)

R. R. P. Singh, P. A. Fleury, K.B. Lyons and P. E. Sulewski, Phys Rev. Lett., **62** (1989) 2736

S. Sugai, S. Shamoto and M. Sato, Phys. Rev. **B38** (1988) 6436

B. M. Wanklyn and B. J. Garrard, J. Mater. Sci. Lett. **2** (1983) 285

E. B. Wilson, J. C. Decius and P. C. Cross, Molecular Vibrations (McGrawn-Hill, New York, 1955)

B. X. Yang, J. M. Tranquada and G. Shirane, Phys. Rev. **B38** (1988) 174

H. J. Zeiger, A. J. Strauss, G. Dresselhaus, Y. C. Liu, P. J. Picone and M. S. Dresselhaus, Phys. Rev. **B40** (1989) 8891

Zhao Min-Guang, Zeng Xiao-Lan, Qian You-Ping, Yi Jun and Zhao Xiao-Ning, J. Phys. **C20** (1987) L917